Restoration of TET2 Function Blocks Aberrant Self-Renewal and Leukemia Progression

Graphical Abstract

Authors

Luisa Cimmino, Igor Dolgalev, Yubao Wang, ..., Aristotelis Tsirigos, Benjamin G. Neel, Iannis Aifantis

Correspondence

luisa.cimmino@nyumc.org (L.C.), benjamin.neel@nyumc.org (B.G.N.), iannis.aifantis@nyumc.org (I.A.)

In Brief

Vitamin C treatment mimics the effect of TET2 restoration on leukemic stem cells and enhances the efficacy of PARP inhibition in suppressing leukemia progression.

Highlights

- *Tet2* restoration reverses aberrant self-renewal of *Tet2*-deficient cells

- *Tet2* restoration promotes DNA demethylation, differentiation, and cell death

- Vitamin C treatment mimics *Tet2* restoration to block leukemia progression

- Vitamin C treatment in leukemia cells enhances their sensitivity to PARP inhibition

Restoration of TET2 Function Blocks Aberrant Self-Renewal and Leukemia Progression

Luisa Cimmino,[1,2,*] Igor Dolgalev,[1,2,3] Yubao Wang,[2] Akihide Yoshimi,[4] Gaëlle H. Martin,[1] Jingjing Wang,[1,2] Victor Ng,[1] Bo Xia,[1] Matthew T. Witkowski,[1,2] Marisa Mitchell-Flack,[1,2] Isabella Grillo,[1,2] Sofia Bakogianni,[1,2] Delphine Ndiaye-Lobry,[1,2] Miguel Torres Martín,[5] Maria Guillamot,[1,2] Robert S. Banh,[2] Mingjiang Xu,[6] Maria E. Figueroa,[5] Ross A. Dickins,[7] Omar Abdel-Wahab,[4] Christopher Y. Park,[1] Aristotelis Tsirigos,[1,2,3] Benjamin G. Neel,[2,8,*] and Iannis Aifantis[1,8,9,*]

[1]Department of Pathology, NYU School of Medicine, New York, NY 10016, USA
[2]Laura & Isaac Perlmutter Cancer Center, NYU School of Medicine, New York, NY 10016, USA
[3]Applied Bioinformatics Laboratories, NYU School of Medicine, New York, NY 10016, USA
[4]Human Oncology and Pathogenesis Program, Memorial Sloan Kettering Cancer Center and Weill Cornell Medical College, New York, NY 10065, USA
[5]Department of Human Genetics, University of Miami, Miller School of Medicine, Miami, FL 33136, USA
[6]Department of Biochemistry and Molecular Biology, University of Miami, Miller School of Medicine, Miami, FL 33136, USA
[7]Australian Center for Blood Diseases, Monash University, VIC 3004, Australia
[8]These authors contributed equally
[9]Lead Contact
*Correspondence: luisa.cimmino@nyumc.org (L.C.), benjamin.neel@nyumc.org (B.G.N.), iannis.aifantis@nyumc.org (I.A.)
http://dx.doi.org/10.1016/j.cell.2017.07.032

SUMMARY

Loss-of-function mutations in *TET2* occur frequently in patients with clonal hematopoiesis, myelodysplastic syndrome (MDS), and acute myeloid leukemia (AML) and are associated with a DNA hypermethylation phenotype. To determine the role of *TET2* deficiency in leukemia stem cell maintenance, we generated a reversible transgenic RNAi mouse to model restoration of endogenous *Tet2* expression. *Tet2* restoration reverses aberrant hematopoietic stem and progenitor cell (HSPC) self-renewal in vitro and in vivo. Treatment with vitamin C, a co-factor of Fe2^{+} and α-KG-dependent dioxygenases, mimics *TET2* restoration by enhancing 5-hydroxymethylcytosine formation in *Tet2*-deficient mouse HSPCs and suppresses human leukemic colony formation and leukemia progression of primary human leukemia PDXs. Vitamin C also drives DNA hypomethylation and expression of a TET2-dependent gene signature in human leukemia cell lines. Furthermore, TET-mediated DNA oxidation induced by vitamin C treatment in leukemia cells enhances their sensitivity to PARP inhibition and could provide a safe and effective combination strategy to selectively target TET deficiency in cancer.

INTRODUCTION

TET2 is one of the most frequently mutated genes in hematopoietic malignancies. Somatic deletions and loss of function mutations in *TET2* are seen in ∼10% of de novo acute myeloid

leukemia (AML), ∼30% of myelodysplastic syndrome (MDS), and almost 50% of chronic myelomonocytic leukemia (CMML) patients (Delhommeau et al., 2009; Kosmider et al., 2009). *TET2* mutations are associated with DNA hypermethylation, increased risk of MDS progression, and poor prognosis in AML (reviewed in Guillamot et al., 2016).

The ten-eleven-translocation (TET1-3) proteins are α-ketoglutarate- and Fe^{2+}-dependent dioxygenases (α-KGDDs) that catalyze the iterative oxidation of 5-methylcytosine (5mC) to 5-hydroxymethylcytosine (5hmC), 5-formylcytosine (5fC), and 5-carboxylcytosine (5caC). These oxidized mCs are key intermediates in DNA demethylation via replication-dependent dilution or base excision repair (BER). Truncations or catalytic domain mutants of TET2, as found in leukemia patients, affect Fe^{2+} and/or α-KG binding, leading to impaired 5mC oxidation and DNA hypermethylation (Pastor et al., 2013; Shen et al., 2014). These findings highlight the importance of targeting aberrant DNA methylation for the treatment of *TET2* mutant diseases.

Several studies have modeled *TET2* loss of function in mice (Guillamot et al., 2016). *Tet2* deletion causes progressive defects in hematopoiesis, including increased hematopoietic stem cell (HSC) self-renewal and myeloid lineage expansion. These phenotypes correlate with loss of 5hmC in hematopoietic stem and progenitor cells (HSPCs), DNA hypermethylation, and altered gene expression consistent with a myeloid lineage bias in self-renewing progenitors. A significant proportion of *Tet2*-deficient mice develop a CMML-like disease, characterized by increased circulating white blood cells (WBCs), monocytosis, and splenomegaly (Moran-Crusio et al., 2011; Quivoron et al., 2011).

TET2 mutations are seen at high allele frequency in CD34^{+} HSPCs (Delhommeau et al., 2009; Papaemmanuil et al., 2016) and in a wide variety of hematopoietic malignancies (Guillamot et al., 2016), suggesting such mutations are early drivers of transformation in cells with multi-lineage potential. *TET2*

mutations are also found in the WBCs of otherwise healthy adults with clonal hematopoiesis, a condition of aging associated with myeloid lineage bias and increased risk of progression to MDS and AML (Sperling et al., 2017). Hence, *TET2* mutation represents a pre-leukemic lesion that can enable disease progression, either by altering the epigenetic landscape or by promoting acquisition of additional oncogenic lesions in aberrantly self-renewing stem cells.

Conceivably, restoring TET2 function could provide therapeutic benefit to patients with clonal hematopoiesis or MDS, but it remains unclear if TET2 deficiency is necessary for disease maintenance. To test this possibility, we generated reversible RNAi transgenic mice to model knockdown and restoration of endogenous *Tet2* in hematopoietic cells. We found that *Tet2* knockdown recapitulates the effects of *Tet2* deletion, leading to aberrant HSC self-renewal and disease. Furthermore, reversing *Tet2* silencing promotes DNA demethylation, cellular differentiation, and cell death, leading to a block in aberrant HSPC self-renewal.

To achieve pharmacological restoration of TET2 activity, we used vitamin C, a co-factor for α-KGDDs. Notably, exogenous vitamin C promotes DNA demethylation in embryonic stem cells (ESCs) and induced pluripotent stem cells (iPSCs) (Chung et al., 2010; Esteban et al., 2010) and dramatically enhances 5hmC levels in a TET-dependent manner (Blaschke et al., 2013; Chen et al., 2013; Yin et al., 2013). Although vitamin C administration has been tested in solid tumors, with some reports of efficacy (Fritz et al., 2014), the possibility that it might act as a targeted therapy to "correct" TET deficiency has not been explored.

Indeed, vitamin C treatment mimics *Tet2* restoration by promoting DNA demethylation and reversing aberrant HSPC self-renewal. Vitamin C administration also impedes CMML progression, myeloid skewing of *Tet2*-deficient hematopoietic cells, and the expansion of primary human AML blasts. Treatment of human AML cell lines with vitamin C increases 5mC oxidation and promotes active demethylation. These events trigger a transient DNA damage response, which, combined with PARP inhibition, increases cell death. Our studies implicate vitamin C, through its ability to enhance TET function, as a potentially non-toxic therapy for TET-associated malignancies.

RESULTS

Generation of Reversible *Tet2* Knockdown Mice

To model reversible *Tet2* knockdown, we generated miR30-based transgenic small hairpin RNA (shRNA) mice that express a doxycycline (Dox)-regulated, fluorescence-linked *Tet2*-specific shRNA (*shTet2*) from the *Col1a1* locus (Premsrirut et al., 2011). The shRNA mice were bred to two transactivator mouse strains: (1) *Vav-tTA* (*VTA*) transgenic mice, which express a pan-hematopoietic, tetracycline-off (Dox-off) tTA transactivator (Kim et al., 2007) (Figure 1A), and (2) *ROSA26-M2rtTA* (*RTA*) tetracycline-on (Dox-on) inducible mice, in which *M2rtTA* expression is driven ubiquitously from the endogenous *ROSA26* promoter (Hochedlinger et al., 2005) (Figure 1B). Compound transgenic shRNA progeny harboring VTA or RTA exhibit Dox-regulated target gene restoration or knockdown, respectively. Transgenic shRNA mice expressing Renilla luciferase-

specific shRNA (*shRen*) were used as negative controls for knockdown and restoration studies (Dow et al., 2014).

Bone marrow (BM), thymus, and spleen RNA from *VTA-shTet2* mice (6- to 8-week-old) showed 50%–70% *Tet2* knockdown by qRT-PCR, compared with *VTA-shRen* controls (Figure 1C). Mice with *Tet2* knockdown developed sustained myeloid lineage bias in peripheral blood (PB) by 6 months of age, and compared with controls, had markedly decreased survival, splenomegaly, and expansion and infiltration of GFP$^+$ cells in spleen and liver (Figures S1A–S1F). At sacrifice, diseased *VTA-shTet2* mice displayed an increased frequency of cKit$^+$ cells in the spleen (Figure S1G) and a predominance of myeloid and erythroid cells. BM Lineage$^-$Sca1$^+$Kit$^+$ (LSK) cells, Lineage$^-$Sca1$^-$cKit$^+$ (cKit$^+$ progenitors), and CD34$^+$ FcR-expressing granulocyte and myeloid progenitors also were increased (Figure S1H). These data are consistent with mouse models of *Tet2* deficiency.

The kinetics of *Tet2* knockdown and restoration were assessed in cohorts of *VTA* and *RTA-shTet2* mice fed Dox food for 28 days (Figure 1D). After 3–7 days of Dox, GFP expression was induced and sustained in the PB of *RTA-shTet2* mice (Figure 1E), whereas complete loss of GFP was detectable after 7–14 days in *VTA-shTet2* mice (Figure 1F). By 3 days of Dox treatment, depletion of *Tet2* mRNA was observed in cKit$^+$ HSPCs (Figure 1G) and immature CD11b$^+$ myeloid lineage cells (Figure 1H) purified from *RTA-shTet2* BM, whereas complete restoration of endogenous *Tet2* levels in *VTA-shTet2* mice was achieved by 28 days.

Tet2 Restoration Reverses Aberrant Self-Renewal

Tet2-deficient HSPCs exhibit increased re-plating capacity in colony-forming assays and a competitive advantage in BM reconstitution studies (Moran-Crusio et al., 2011; Quivoron et al., 2011). To ask if sustained loss of *Tet2* function is required for aberrant stem cell self-renewal, we first performed serial re-plating assays of *VTA-shTet2* colony-forming cells in methylcellulose medium (Figure 2A). Colonies from *VTA-shTet2* (*Tet2*-knockdown) BM were re-plated successively until aberrant self-renewal was observed and then placed in methylcellulose media with or without Dox. Consistent with previous studies comparing wild-type and *Tet2*-deficient BM cells, control *VTA-shRen* colonies did not re-plate beyond three passages (P3), while *Tet2* knockdown (*VTA-shTet2*) colonies replated for up to four passages (P4) (Figure 2B). Re-plating for a fifth passage (P5), in the presence of Dox to turn off the expression of *shTet2*, caused a block in colony-forming capacity, loss of GFP expression (Figures 2C and 2D), and a 2-fold increase in *Tet2* mRNA levels (Figure 2E).

We next assessed the effect of *Tet2* restoration in the context of oncogenes that cooperate with *Tet2* deficiency and accelerate leukemia onset, such as *AML-ETO9a* and *FLT3-ITD* (Rasmussen et al., 2015; Shih et al., 2015). *RTA-shTet2* cKit$^+$ cells transduced with an *AML-ET09a-IRES-mCherry* (*AE9aC*)-expressing retrovirus or total BM cells from *Flt3-ITD; RTA-shTet2* mice were serially re-plated in methylcellulose. *Tet2* knockdown increased the re-plating capacity of *AE9aC*-expressing (Figure S2A) and *Flt3-ITD*-expressing (Figure S2B) cells, whereas *Tet2* restoration impaired re-plating (Figures S2C–S2F) and promoted myeloid differentiation (Figures S2G and S2H).
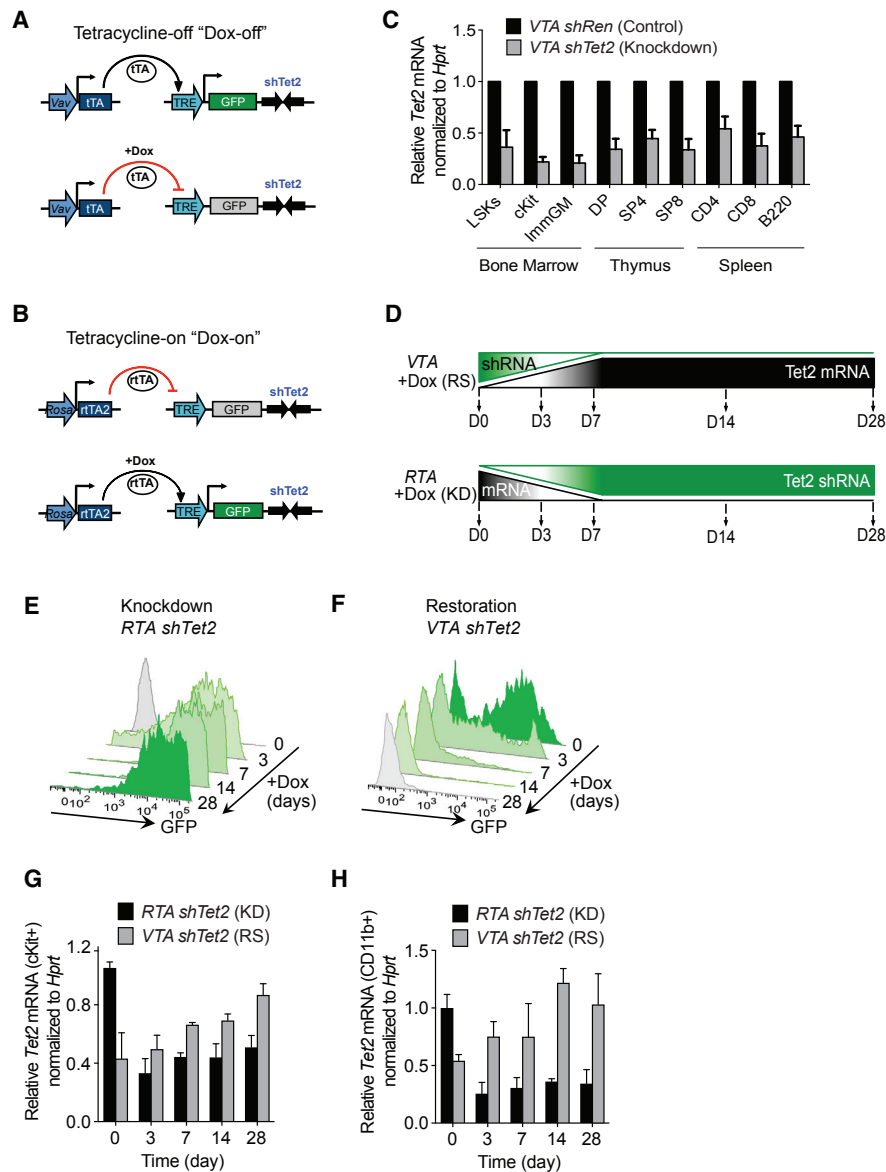
Figure 1. Generation of Inducible and Reversible Tet2 Knockdown Mice

(A) Schematic representation of *Vav-tTA*-driven (*VTA*) reversible *Tet2* knockdown mice.

(B) Schematic representation of *Rosa-rtTA*-driven (*RTA*) inducible *Tet2* knockdown mice.

(C) *Tet2* mRNA levels (normalized to *Hprt*) in bone marrow, thymus, and spleen cells from *VTA shTet2* mice, compared with cognate cells from *VTA shRen* control mice.

(D) Schematic representation of *Tet2* restoration (RS) versus knockdown (KD) in mice treated with doxycycline (Dox) food for 28 days (D0–D28).

(E and F) Representative flow cytometric analysis of GFP in peripheral blood cells of Dox-regulated *RTA shTet2* inducible knockdown (E) mice and following *Tet2* restoration in *VTA shTet2* mice (F).

(G and H) *Tet2* mRNA expression (normalized to *Hprt*, relative to *RTA shTet2* at day 0) in cells isolated from *RTA shTet2* and *VTA shTet2* mice treated with Dox food to compare knockdown (KD) or restoration (RS), respectively, in cKit⁺ bone marrow cells (G) and CD11b⁺ immature myeloid cells (H) (n = 4–5 mice per group). See also Figure S1.

To determine the effect of *Tet2* restoration on HSC self-renewal in vivo, we performed competitive bone marrow transplantation (BMT) assays. As reported previously for *Tet2*$^{+/-}$ and *Tet2*$^{-/-}$ BM, *Tet2* knockdown cells displayed a competitive advantage (Figure S2I) and a myeloid lineage bias in donor PB (Figure S2J). Beginning at 6 weeks post-transplant, Dox food was administered to half of the cohort, and treated and untreated mice were monitored for donor chimerism for up to 28 weeks. *VTA-shRen* donor frequency in PB remained unchanged upon Dox treatment (Figure 2F), whereas Dox-treated *VTA-shTet2*
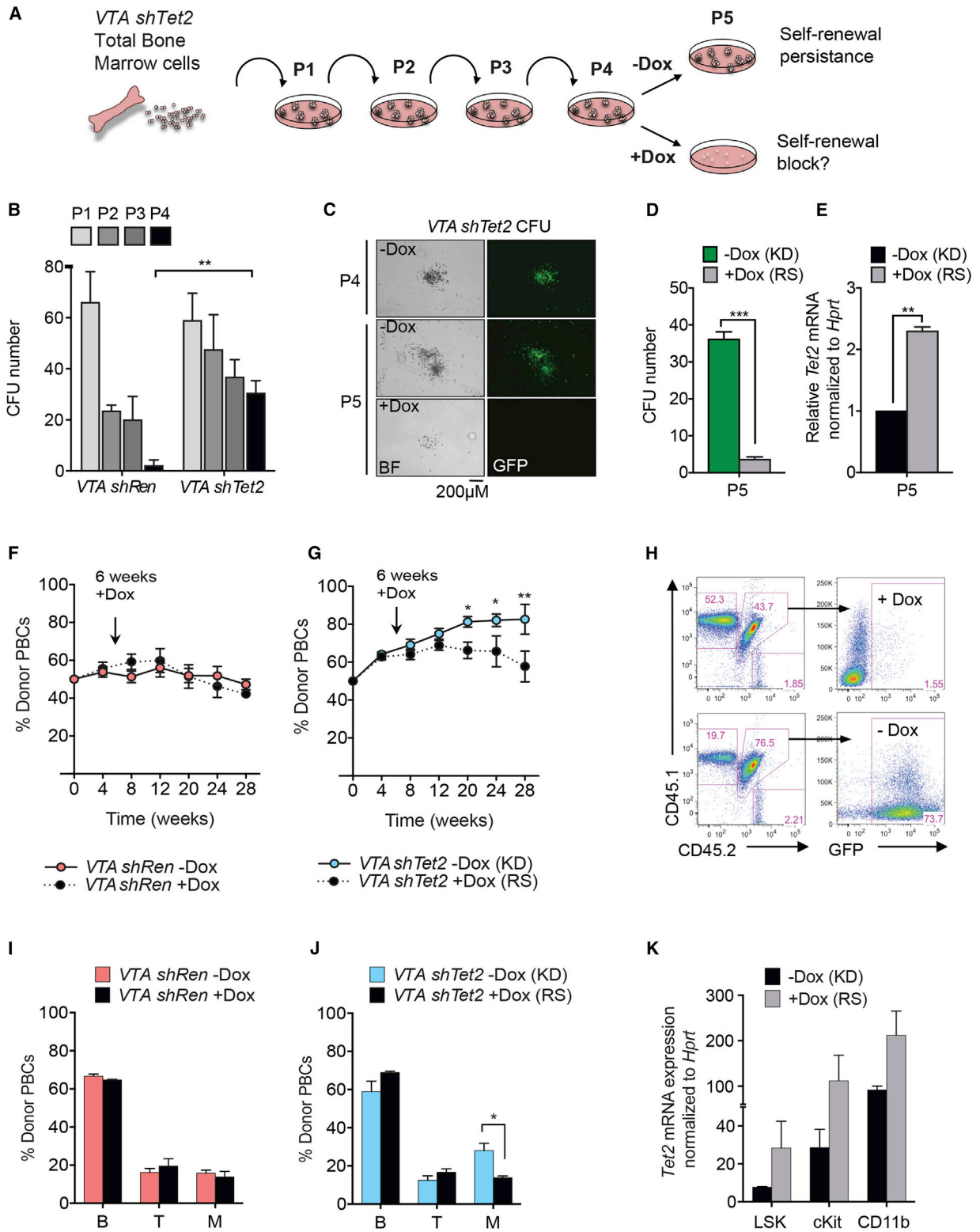
Figure 2. *Tet2* Restoration Blocks Aberrant Hematopoietic Stem Cell Self-Renewal In Vitro and In Vivo

(A) Schematic of colony-forming assays performed with *Tet2* knockdown cells. After re-plating for four successive passages (P1–P4), *VTA shTet2*-expressing cells are treated with Dox to determine the effects of *Tet2* restoration on re-plating.

(legend continued on next page)

recipients showed a significant loss of competitiveness from 20 weeks post-transplant (Figure 2G), which correlated with loss of fluorescence-coupled shRNA expression (Figure 2H). Dox treatment also reversed the myeloid lineage bias caused by *Tet2* knockdown in *VTA shTet2* donor PB (Figures 2I–2J). Administering Dox from the day of transplant (0 weeks), or pre-treating donor mice with Dox for 4 weeks prior to BMT (−4 weeks), was even more effective at blocking the competitive advantage of *VTA-shTet2* knockdown cells upon restoration than treatment beginning at 6 weeks or 12 weeks post-transplant (Figures S2K and S2L). Significant loss of donor chimerism upon *Tet2* restoration was observed in all stem and progenitor cell compartments and in myeloid lineage cells of the BM and spleen (Figure S2M). These effects correlated with an ~2-fold increase in *Tet2* expression in sorted populations of donor LSK, cKit^{+} progenitors, and immature CD11b^{+} cells (Figure 2K). Therefore, sustained *Tet2* deficiency is required to maintain aberrant HSC self-renewal, and its effects are reversed upon *Tet2* restoration.

Tet2 Restoration Promotes Myeloid Differentiation and Cell Death in HSPCs

To study how *Tet2* restoration influences HSC function, we generated inducible cKit[+] *Tet2* knockdown cell lines in cytokine-containing media. Inducing *Tet2* knockdown in *RTA-shTet2* cKit^{+} cells over a 2-week period led to reduced *Tet2* mRNA levels (2- to 2.5-fold), compared with those in control *RTA-shRen* cells (Figures S3A and S3B). *Tet2* expression was restored completely 10–14 days following Dox-withdrawal (Figures 3A, S3C, and S3D). Similar kinetics of *Tet2* restoration were observed in Dox-treated *VTA-shTet2* cells (Figures S3E and S3F). Restoring *Tet2* caused a block in cell proliferation (Figures 3B, S3G, and S3H), due to an increase in annexinV^{+} apoptotic cells (Figure 3C) and a delay in cell-cycle progression (Figures S3I and S3J).

Tet2 knockdown cells in culture expressed cKit, Sca1, and CD34 on their surface in addition to low expression of the SLAM markers CD150 and CD48, but were negative for FcR and the myeloid lineage markers Gr1 and CD11b (Figure S3K). Upon prolonged *Tet2* restoration (Days 18 and 21), a slight decrease in cKit[+] surface expression was detected, while CD11b and CD34 expression increased modestly (Figures 3D and 3E). Increased CD34 expression is associated with loss of long-term self-renewal potential in mouse HSCs (Wilson et al.,

2008), and *Tet2* has been shown to facilitate the expression of myeloid-specific genes such as Mac1/CD11b in B cells undergoing CEBPα-induced *trans*-differentiation (Kallin et al., 2012). Hence, these data suggest that loss of aberrant self-renewal capacity in *Tet2*-restored cells is associated with impaired proliferation, increased cell death, and priming toward myeloid differentiation.

Differential Methylation Correlates with Global Transcriptional Changes upon *Tet2* Restoration

Steady-state *Tet* deficiency, modeled in mouse ESCs and HSCs, is associated with genomic loss of hydroxymethylation and DNA hypermethylation (Pastor et al., 2013). Similarly, significant DNA hypermethylation (gain of 5mC) and decreased hydroxymethylation (loss of 5hmC) was induced upon *Tet2* knockdown in HSPCs (Figure S3L). Conversely, DNA demethylation (~30% loss of total 5mC) was observed after 7–10 days of *Tet2* restoration in cKit[+] *Tet2*-knockdown cells (Figure 3F); concomitantly, 5hmC levels increased 10–14 days after restoration to almost 2-fold those of knockdown levels (Figure 3G). These findings are consistent with a role for TET2 in promoting DNA demethylation. Interestingly, global methylation levels were restored after 14 days despite peak *Tet2* restoration; these regions of the genome could represent newly methylated loci in combination with higher levels of 5hmC.

TET family members can promote gene activation or repression (Pastor et al., 2013; Shen et al., 2014), and these transcriptional alterations are coupled to altered DNA methylation across gene bodies, enhancers, and at the boundaries of DNA methylation canyons (Rasmussen et al., 2015; Wiehle et al., 2015). To identify the locus-specific changes in DNA methylation upon *Tet2* restoration, we performed single base resolution reduced representative bisulfite sequencing (RRBS) (Gu et al., 2011). Differentially methylated cytosines (DMCs) either gained or lost methylation and were most abundant after 10 days of *Tet2* restoration (Figures 4A and S4A). Differentially methylated regions (DMRs) exhibited greater losses than gains in methylation at CpG shores (>2 kb distance from CpG islands) and across exons and introns, suggesting loss of DNA methylation specifically within gene bodies (Figure 4B). Determining which genomic regions are direct targets of TET2 in primary hematopoietic cells by chromatin-binding studies has been hindered by the lack of antibodies that recognize endogenous TET2. However, by using a TET2 chromatin

(B) Total number of colony-forming units (CFU) generated by *VTA shRen* control or *VTA shTet2* knockdown cells. Data are representative of three experiments (mean + SD), **p < 0.005.
(C) Representative appearance of colonies generated after 4 passages (P4) with *Tet2* knockdown re-plated ± Dox from P4–P5.
(D) Number of CFUs from passage 5 (P5) *Tet2* knockdown (KD) and *Tet2*-restored (RS) cells.
(E) *Tet2* mRNA levels normalized to *Hprt* in RS cells relative to KD from (D). Mean + SEM from 3 experiments is shown, **p < 0.005 and ***p < 0.005.
(F and G) Donor peripheral blood cell (PBC) percentage in mice subjected to competitive bone marrow reconstitution and given Dox food from 6 weeks post-transplant of *VTA shRen* control (F) or *VTA shTet2* donor bone marrow cells (G).
(H) Representative flow cytometric analysis of donor chimerism and GFP expression in *VTA shTet2*-transplanted mice ± Dox treatment at 28 weeks post-transplant.
(I and J) Representation of donor PBCs in the indicated hematopoietic lineages 28 weeks post-transplant in mice with *VTA shRen* (I) or *VTA shTet2* (J) bone marrow cells ± Dox treatment.
(K) *Tet2* mRNA levels, normalized to *Hprt* expression, in *Tet2* KD or *Tet2* RS cells isolated from *VTA shTet2*-reconstituted mice at 28 weeks post-transplant. Mean + SEM is shown (n = 4–5 mice per group). *p < 0.05, **p < 0.005.
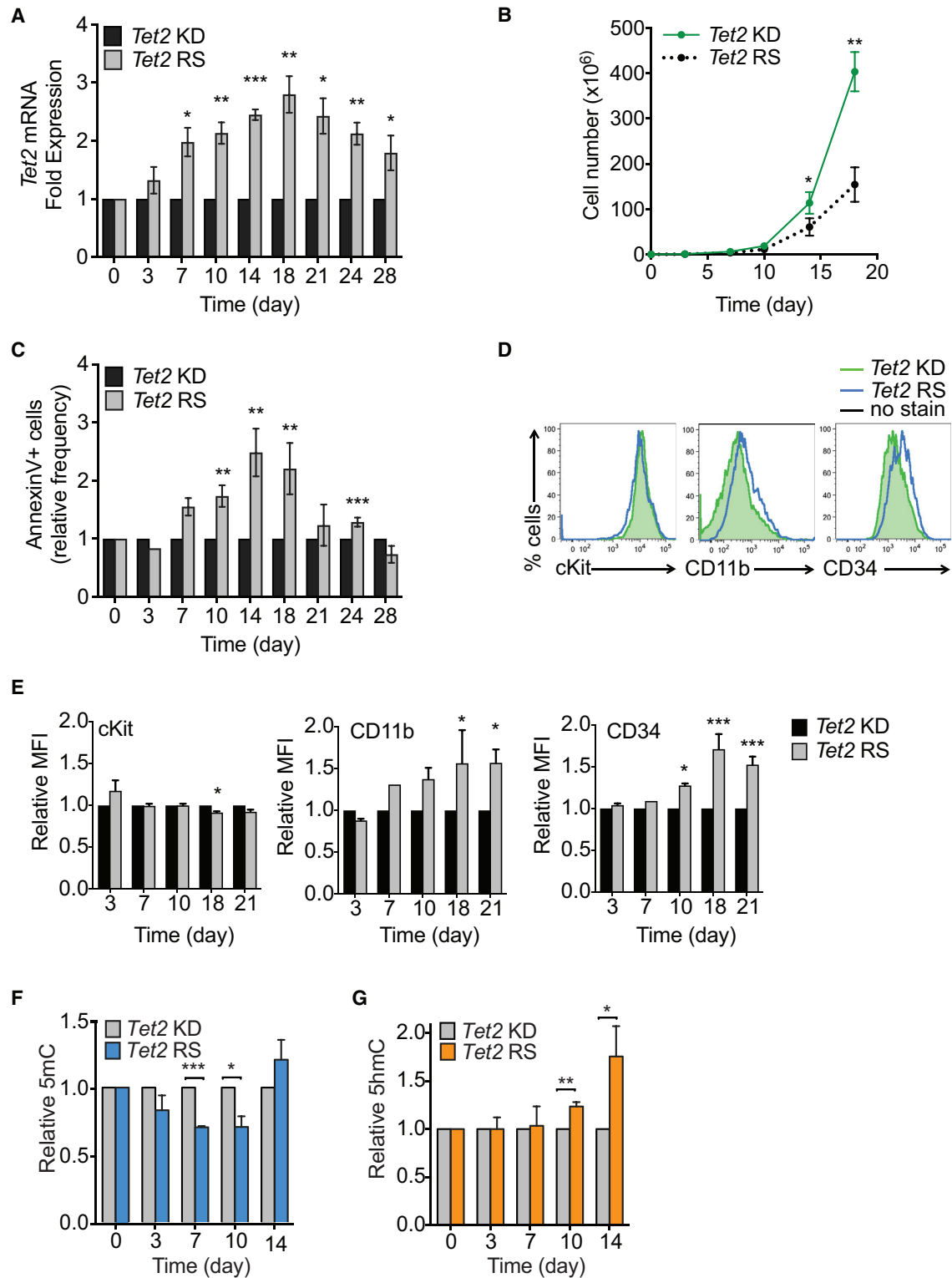See also Figure S2.

Figure 3. *Tet2* Restoration Promotes DNA Demethylation, Differentiation, and Cell Death

(A–E) Effects of *Tet2* restoration on *Tet2* mRNA levels, proliferation, survival, and differentiation of cKit+ cells. *Tet2* mRNA levels (normalized to *Hprt*) in cKit+ cells grown in liquid culture for 28 days with sustained *Tet2* knockdown (KD) or inducible restoration (RS) upon Dox administration (A). Proliferation (B) and apoptosis, as assessed by Annexin V staining (C), of *Tet2* RS versus sustained *Tet2* KD cells. Representative flow cytometry histograms of stem and progenitor (cKit and

(legend continued on next page)

immunoprecipitation sequencing (ChIP-seq) signature generated by overexpressed, flag-tagged TET2 in mouse erythroid leukemia cells (Pan et al., 2017), we found that at day 10 of restoration, TET2-bound DMRs were highest at promoters, exons, and CpG shores, with CpG island DMRs enriched for TET2 binding from days 7–14 of restoration (Figures S4B and S4C).

Transcriptomic analysis revealed a strong bias toward upregulation of genes (n = 173) as opposed to gene downregulation (n = 15), with >2-fold changes (p < 0.05) after 10 days of *Tet2* restoration (Figures 4C and 4D). This bias correlated with the peak in differential methylation observed at day 10 of *Tet2* restoration (Figures 3G and 4A). The tendency toward greater downregulation of gene expression by 14 days of restoration might reflect a slowing of cell proliferation or activation of cell death in response to a threshold level of *Tet2* achieved by 10 days of restoration (Figures 4E and 4F).

Tet2 Restoration Drives Loss of Aberrant DNA Methylation and Expression of Myeloid Differentiation Genes

Gene set enrichment analysis (GSEA) revealed that genes upregulated upon 14 days of restoration included cytoskeletal regulators that are highly expressed in differentiated myeloid lineage cells, including Ras homolog gene family, member C (*RhoC*) and Ras and Rab interactor 2 (*Rin2*), the epigenetic regulator DNA-methyltransferase 3b (*Dnmt3b*), and the transcription factor early B cell factor-1 (*Ebf1*). Conversely, genes important for cytokine signaling, such as the Map kinase family member *Map3k14*, were downregulated (Figure 4G). Ingenuity Pathway Analysis revealed apoptosis, death receptor signaling, and DNA damage response pathways (p53 signaling) to be specifically upregulated at 10 days of restoration (Figure S4D). These pathways might reflect active DNA demethylation as the primary response to *Tet2* restoration in these cells, despite a peak in 5hmC levels by 14 days of restoration.

TET2 mutant leukemia patients exhibit DNA hypermethylation, and distinct AML subtypes can be identified by their unique methylation signatures (Figueroa et al., 2010). By 14 days of *Tet2* restoration, the mouse orthologs of genes hypermethylated in AML patients tended to be upregulated; conversely, genes hypomethylated in AML were downregulated. Specifically, 5/7 unique gene clusters that are aberrantly hypermethylated in subtypes of AML compared with normal human CD34^{+} cells were significantly upregulated (false discovery rate [FDR] <0.25) following *Tet2* restoration (Figures 4H and 4I; Table S1). Upregulated genes included those hyper-methylated in patients with *AML1-ETO* (t(8;21)) or *PML-RAR* translocations or bearing *CEBPA* mutations (Table S1).

Vitamin C Treatment Mimics Effects of *Tet2* Restoration

Our findings suggested that TET2 restoration could provide a novel therapeutic strategy to target *TET2* mutant cells in patients with clonal hematopoiesis, MDS, or AML. As genetic restoration is not an option in patients, we sought to pharmacologically augment TET activity. Vitamin C is a co-factor of α-KGDDs and can increase 5hmC and promote TET-dependent DNA demethylation (Young et al., 2015). Biochemical studies suggest that vitamin C binds TET2 and acts as a targeted electron donor to restore iron to the Fe^{2+} state in the TET catalytic cycle, thereby increasing the rate of 5mC oxidation by up to 8-fold (Yin et al., 2013). We hypothesized that vitamin C treatment, by increasing TET catalytic activity, might pharmacologically mimic *Tet2* restoration in *Tet2*-deficient HSCs.

Treatment of wild-type Lin[−]cKit[+] cell cultures with vitamin C (L-ascorbic acid [L-AA]) led to a 2-fold increase in 5hmC and a 2-fold loss in 5mC in genomic DNA, as measured by dot blot analysis (Figure 5A). Moreover, whereas $Tet2^{+/-}$ or $Tet2^{-/-}$ cells showed aberrant re-plating capacity (>4 passages) when treated with PBS, vitamin C-treated cells showed a severe block in re-plating capacity (Figure 5B). Importantly, vitamin C did not affect colony formation by wild-type cells. High levels of vitamin C can lead to reactive oxygen species (ROS) production via the Fenton reaction (Du et al., 2012). However, serial re-plating capacity was still blocked when catalase, an enzyme that can decompose hydrogen peroxide (H_2O_2) to water and oxygen, was included with vitamin C in the media (Figure 5C).

There are multiple members of the α-KGDD family, and most, if not all of these, use vitamin C as a co-factor (Young et al., 2015). Although the ability of vitamin C to suppress re-plating correlated with increased 5hmC and decreased 5mC levels in DNA, these findings alone do not establish that vitamin C affects self-renewal via TET family members. Notably, $Tet2^{-/-}$ cells were somewhat resistant to the effects of vitamin C, yet still showed decreased re-plating compared with untreated cells (Figure 5D). Conceivably, other TET family members compensate for the absence of *Tet2* and mediate the effects of vitamin C on $Tet2^{-/-}$ cells; alternatively, vitamin C could act through other α-KGDDs. *Tet2* and *Tet3* are the most abundantly expressed *Tet* genes in HSPCs (An et al., 2015). We therefore performed colony-forming assays with BM cells from $Tet2^{+/-}$, $Tet2^{-/-}$, and $Tet2^{-/-}Tet3$-knockdown, the latter generated by crossing $Tet2^{-/-}$ mice to *RTA* transgenic *shTet3* mice ($Tet2^{-/-}Tet3^{KD}$). $Tet2^{-/-}Tet3^{KD}$ cells exhibited increased re-plating capacity (Figure S5A), comparable to $Tet2^{+/-}$ and $Tet2^{-/-}$ cells. However, $Tet2^{-/-}Tet3^{KD}$ cells were far more resistant than $Tet2^{-/-}$ cells to the inhibitory effect of vitamin C on serial re-plating (Figures 5D and S5A). Furthermore, vitamin C-evoked 5hmC generation was markedly impaired in $Tet2^{-/-}Tet3^{KD}$ cKit^{+} cells (Figure 5E), consistent with the significantly decreased *Tet2* and *Tet3* mRNA levels in

---

CD34) or differentiation (CD11b) marker expression upon *Tet2* KD or *Tet2* RS after 21 days in culture (D). Quantification of GFP by relative mean fluorescence intensity (MFI) is shown (E).

(F and G) Global changes in methylation were measured in genomic DNA isolated from cKit^{+} cells during inducible *Tet2* RS, and compared to cells with sustained *Tet2* KD. Quantification was performed using ELISAs for 5mC (F) and 5hmC (G). Mean ± SEM is shown for 2 biological replicates, performed in triplicate. *p < 0.05, **p < 0.005, and ***p < 0.005.

See also Figure S3.
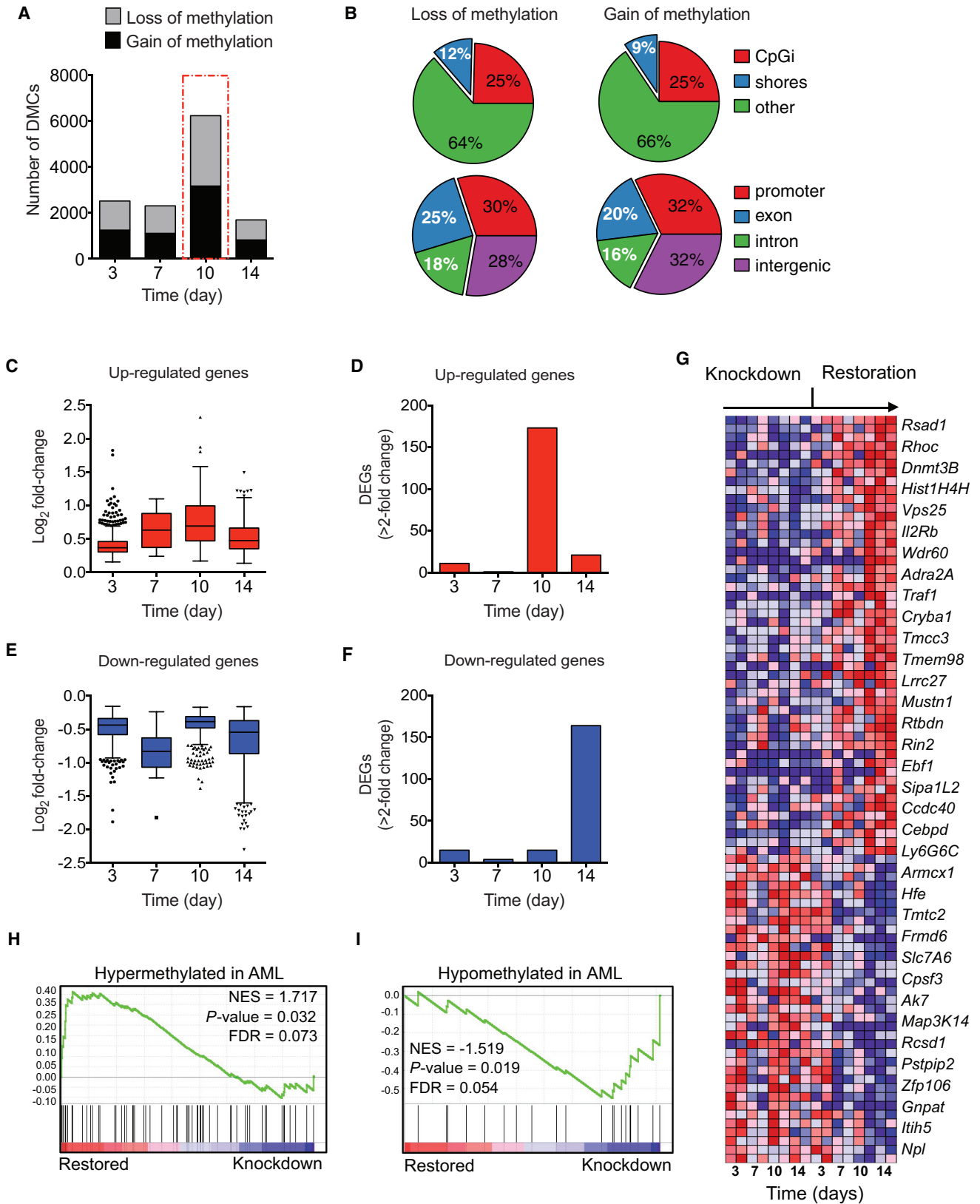
(legend on next page)

Tet2^{−/−}*Tet3*[KD] cells (Figure 5F). Together, these data suggest that vitamin C blocks aberrant HSPC self-renewal primarily by increasing TET2 and TET3 activity.

Vitamin C is an essential dietary requirement in humans, due to mutation in the enzyme L-gulonolactone oxidase, which remains functional in mice (Young et al., 2015). Despite being able to generate vitamin C in the absence of dietary supplementation, mice deficient in *Tet2* still develop myeloid malignancies that mimic human disease. This finding suggests that supra-physiological doses of vitamin C might be required in vivo to block *TET2* mutant hematopoietic neoplasia. Previous pharmacokinetic studies showed that administration of vitamin C as sodium ascorbate (ASC) by intraperitoneal (i.p.) injection in mice can increase plasma levels from approximately 10 μM up to 30 mM for 10–30 min and remain >200 μM for up to 4 hr (Yun et al., 2015). To ask if high-dose vitamin C could induce 5hmC production in vivo, we injected a cohort of mice with a single dose of ASC (4 g/kg). Flow cytometric analysis of 5hmC in PB revealed an increase in 5hmC that remained ~2-fold above baseline levels for 2–6 hr post-injection (Figure 5G). We then tested the effect of daily injections of ASC for 3 successive days and again found 5hmC levels to be higher than baseline, with a 2-fold loss in 5mC in PB (Figure S5B).

As *Tet2* restoration blocks myeloid disease progression following BMT, we treated mice reconstituted with *Tet2*^{+/+} or *Tet2*^{−/−} BM with i.p. injections of PBS or ASC for 24 weeks (Figure S5C). As expected, compared with *Tet2*^{+/+} recipients, *Tet2*^{−/−} mice developed CMML-like disease with elevated WBC counts from 12 weeks post-transplant in the PBS-injected group that increased progressively to 24 weeks. Remarkably, and consistent with its effects in vitro, ASC treatment significantly decreased WBC counts (Figure 5H) and CMML progression in *Tet2*^{−/−} mice. Minor decreases in WBC counts were also observed in ASC-injected *Tet2*^{+/+} recipients. The decrease in *Tet2*^{−/−} WBCs upon ASC treatment correlated with a diminished frequency of myeloid lineage donor cells (Figure 5I) and decreased numbers of circulating myeloid cells in PB (Figure 5J).

Next, we performed colony-forming and liquid differentiation assays with purified leukemic HSPCs and blasts from three *TET2* mutant patients (Table S2). Similar to our observations on *Tet2*-deficient mouse cells, patient-derived HSPCs and blasts showed decreased clonogenicity in methylcellulose assays (Figure S5D) and increased surface expression of the myeloid marker CD14 in liquid culture upon treatment with vitamin C (Figure S5E).

We also evaluated the effects of ASC on two primary human AML PDX models (Table S2). Upon detection of >1% human CD45+ (hCD45+) cells in PB, mice were treated i.p. with PBS or ASC (Figure S5F). Circulating hCD45+ cells in PB, spleen weight, and blast frequency in BM and spleen were all reduced in ASC-treated PDXs, compared with PBS controls (Figures S5G–S5J). These data suggest that high-dose vitamin C treatment could be effective for preventing myeloid disease progression.

## Vitamin C Increases TET Activity in Human AML Cells and Drives DNA Hypomethylation

The ability of vitamin C to block self-renewal and myeloid disease progression in mice prompted us to explore its effects on TET function and 5hmC generation in the HL60 and MOLM13 cell lines, representative of acute myeloblastic and acute monocytic leukemia, respectively (Table S3). These cell lines do not harbor TET mutations (Barretina et al., 2012) but were shown to be sensitive to vitamin C treatment in a previous study (Kawada et al., 2013); however, a mechanistic role for TET activity and 5hmC in the effects of vitamin C was not explored. Consistent with our observations using mouse HSPCs, vitamin C treatment for 72 hr caused increased 5hmC formation in both lines (Figure 6A), without altering *TET1-3* expression (Figure S6A). We performed 5hmC DNA immunoprecipitation (5hmeDIP) with genomic DNA from untreated HL60 cells (0 hr) and cells treated for 72 hr with vitamin C. Nearly all differentially hydroxymethylated peaks (29,492; 97%) exhibited gain of 5hmC upon vitamin C treatment (Figure 6B). Increased 5hmC was enriched within gene bodies, compared with transcription start sites (TSS) or transcription end sites (TES) (Figure 6C), and in the center of CpG islands and at CpG shores (+/− 3 kb) (Figure S6B). Traditional bisulfite sequencing does not distinguish between 5mC and 5hmC. Therefore, we performed oxidative RRBS (oxRRBS), which first converts 5hmC to 5fC and, after bisulfite treatment and sequencing, allows comparative DNA methylation changes to be quantified specifically at 5mC sites (Booth et al., 2013). We observed a 2-fold loss in 5mC by 72 hr of vitamin C treatment in both leukemia cell lines (Figures 6D and S6C). DMRs were distributed almost identically in the two lines, with 50% located within CpG islands and shores and >70% associated with gene bodies and promoters (Figure 6E). Greater loss than gain in 5mC was observed across almost all chromosomes (Figure 6F) with 1.5- to 2-fold greater loss in 5mC in all CpG contexts and genomic loci (Figure 6G).

Figure 4. Differential Methylation and Global Transcriptional Changes upon *Tet2* Restoration

(A and B) Reduced representation bisulfite sequencing (RRBS) of DNA from cKit+ cells in vitro, showing the number of differentially methylated cytosines (DMCs) (q < 0.05, DiffMeth >10%) (A) and the distribution of differentially methylated regions (DMRs) according to CpG context and genomic location (B) at 10 days of *Tet2* restoration (q < 0.05, DiffMeth >10%, 500 bp window).

(C–F) Distribution of differentially expressed genes (DEGS, p < 0.05) in cKit+ cells subjected to *Tet2* restoration for the indicated times. The average log2 fold-changes in all upregulated genes (C) with >2-fold change in expression (D) and in all downregulated genes (E) with >2-fold change in expression (F) are shown.

(G–I) Gene-expression analysis and gene set enrichment analysis (GSEA). Heatmap shows a subset of differentially expressed genes in cKit+ cells subjected to *Tet2* restoration for the indicated times (G). GSEA plots of genes hypermethylated in AML patients that are upregulated in *Tet2* restored cells (H) or hypomethylated genes in AML patients that are downregulated upon *Tet2* restoration (I) (related to Table S1). Decreased gene expression is indicated by shades of blue; increased expression is indicated by shades of red. RRBS and RNA-seq were performed on 2 replicates per time point. *p < 0.05, **p < 0.005, and ***p < 0.005.

See also Figure S4.
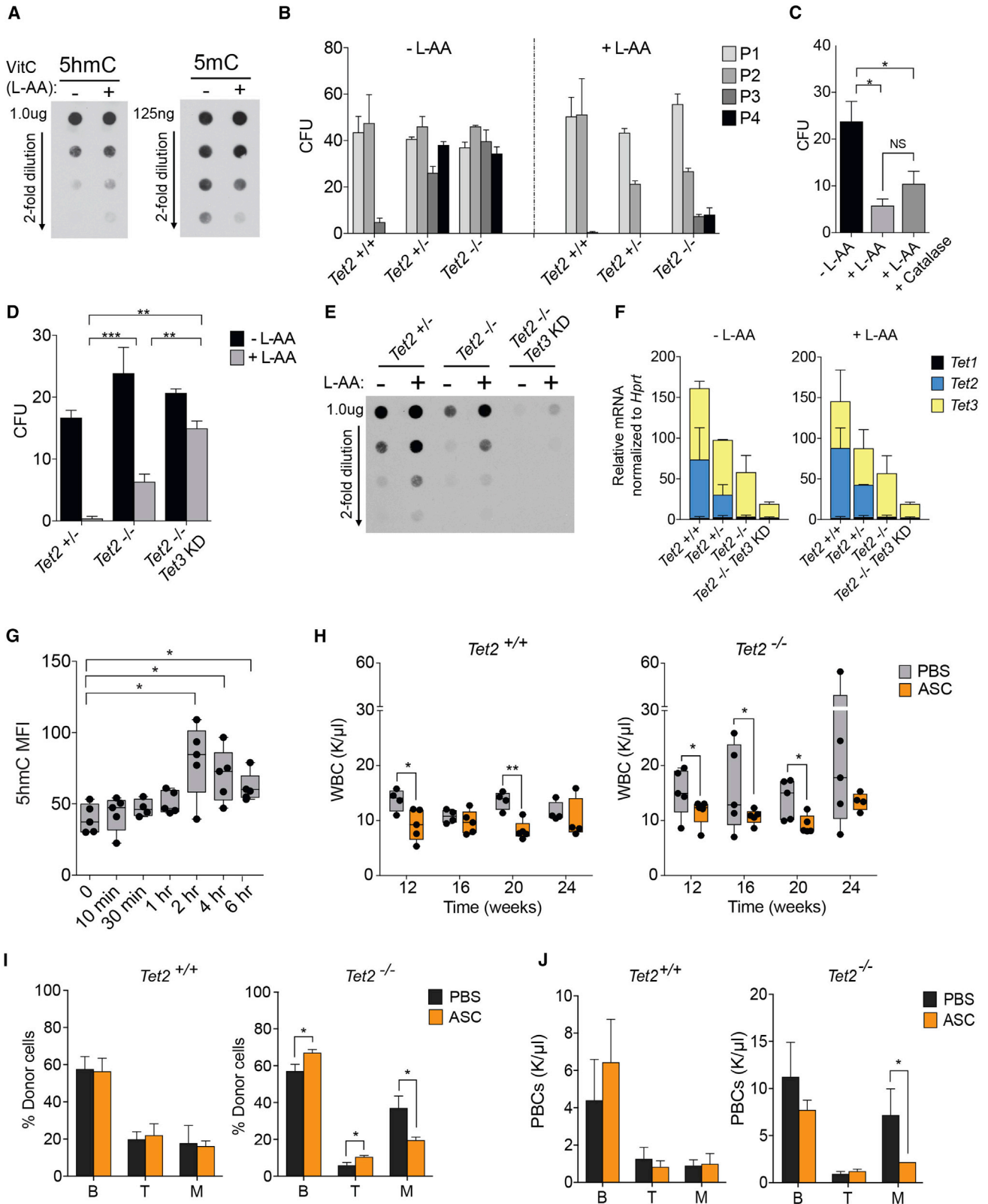
(legend on next page)

Transcriptomic analysis revealed strong overlap in the vitamin C-regulated genes in HL60 and MOLM13 cells after 12 hr of treatment (Figure S6D), although there was less overlap at 72 hr (Figure S6E). Nevertheless, there was enrichment for *Tet2*-restored genes from mouse cKit⁺ cells following 12 hr of vitamin C treatment of both human leukemia lines (Figure S6F), which remained significant in MOLM13 cells at 72 hr (Figures 6H and S6G). Fourteen out of 50 (14/50) genes upregulated by *Tet2* restoration in mouse cKit⁺ cells also were induced in both human leukemia lines after 12 hr of vitamin C treatment, including genes involved in apoptotic and death receptor signaling (*BAX, GADD45a*), phosphatidylcholine biosynthesis (*CHKA* and *CHKB*), and NOTCH signaling (*PSENEN*) (Figure 6I). Of the top genes downregulated by *Tet2*-restoration, 34/50 were downregulated in both leukemia lines after 12 hr of vitamin C (Figure S6H). Hence, vitamin C treatment can enhance TET2 function in human leukemia cells in a manner similar to the effects of *Tet2* restoration in mouse HSPCs.

TET-Mediated Oxidation of DNA by Vitamin C in Combination with PARP Inhibition Enhances AML Cell Death

We observed significant decreases in cell viability of *Tet2*⁺/⁻, *Tet2*⁻/⁻, and *Tet2*⁻/⁻*Tet3*^KD mouse cKit⁺ cells during liquid culture (2 weeks) in the presence of increasing concentrations of vitamin C (Figure S7A). As seen in colony-forming assays, vitamin C had less effect on the viability of *Tet2*⁻/⁻ and *Tet2*⁻/⁻*Tet3*^KD cells in liquid culture compared with *Tet2*⁺/⁻ cells. Remarkably, *Tet2* restoration or vitamin C treatment of *AML-ETO9a*-expressing or *FLT3-ITD*-expressing, *Tet2* knockdown cells also impaired their proliferation in liquid culture (Figures S7B and S7C). We therefore extended our analysis of the effects of vitamin C on 5hmC formation and cell viability to a panel of human myeloid leukemia lines, including (in addition to HL60 and MOLM13) K562 (blast crisis chronic myeloid leukemia), THP1 (acute monocytic leukemia), and KG-1 and KASUMI-1 (acute myeloblastic leukemias) (Table S3). Vitamin C caused decreased viability after 72 hr of treatment in all cell lines (Figure 7A) without any change in TET1-3 expression (Figure S7D). The effects on proliferation increased at higher vitamin C concentrations (up to 1 mM), but there was a substantial decrease in viability even at lower doses (125 μM) when cells were treated for up to 2 weeks (Figure S7E).

Levels of 5hmC increased in DNA from all human leukemia cells tested in response to vitamin C treatment for 72 hr (Figure 7B). Although 5hmC is a stable modification, its iterative oxidation products, 5fC and 5caC, recruit the BER machinery and are actively removed by thymidine DNA glycosylase (TDG) (Shen et al., 2014). Notably, vitamin C-treated human AML cells exhibited 5fC depletion, changes in 5caC levels and loss of 5mC (Figure 7C), suggestive of active DNA demethylation by BER. As noted above, vitamin C can generate increased H_2O_2, which could promote oxidative DNA damage and trigger DNA repair (Cadet and Wagner, 2013). However, 2-phospho-L-ascorbic acid (P-AA), which does not generate ROS (Du et al., 2012), also induced 5hmC formation and cell death in AML cells (Figures S7F and S7G). Moreover, vitamin C (at 250 μM or 1 mM) did not increase dichlorofluorescein (DCF) fluorescence, an indicator of intracellular ROS (Figure S7H).

Poly ADP ribose polymerase (PARP) is an essential mediator of BER that targets single-strand breaks (SSBs) induced by DNA damage and recruits BER complex proteins (Morales et al., 2014). The peak of DNA demethylation upon 10 days of *Tet2* restoration to cKit⁺ cells correlated with increased expression of *Parp* and *Gadd45* (Figure 7D), whose gene products function in DNA demethylation (Barreto et al., 2007; Ciccarone et al., 2012). As noted above, *Tet2* restoration also evoked a p53 transcriptional signature, consistent with a DNA damage response (Figure S4D). We therefore compared the expression of *PARP*, *GADD45*, and additional genes involved in BER and active DNA demethylation, including DNA glycosylases (*MBD4*, *UNG*, *TDG*, *SMUG1*, *MUTYH*), ligases (*NEIL1/2*), endonucleases (*APEX1/2*, *FEN1*), and polymerases (*POLD*β, *POLD1/2*) in vitamin C-treated human AML cells. Indeed, BER genes such as *PARP* and *GADD45* were upregulated in HL60 (Figure 7E) and MOLM13 cells (Figure 7F), indicating that *Tet2* restoration and vitamin C treatment induce the expression of genes whose products mediate active DNA demethylation.

PARP inhibition can increase tumor sensitivity to DNA damage induced by chemotherapy and results in synthetic lethality in cells lacking intact BER or harboring homologous recombination (HR) defects (Morales et al., 2014). We hypothesized that TET-mediated DNA oxidation induced by vitamin C could render AML cells hypersensitive to PARP inhibition by blocking DNA repair associated with DNA demethylation. To test this possibility, we treated AML cell lines with combinations of the PARP

Figure 5. Vitamin C Treatment Mimics *Tet2* Restoration in Hematopoietic Stem Cells and Blocks Myeloid Disease Progression

(A) DNA dot blots for 5hmC and 5mC in genomic DNA from primary mouse cKit⁺ cells treated with 250 μM vitamin C (L-ascorbic acid, L-AA) for 6 days. Data are representative of 2 experiments.

(B–D) Colony-formation assays with *Tet2*⁺/⁺, *Tet2*⁺/⁻, and *Tet2*⁻/⁻ bone marrow cells treated with L-AA. Cells were re-plated for four passages (P1–P4) (B), *Tet2*⁻/⁻ CFUs re-plated from passage 4 to 5 (P4–P5) ± catalase (C), and *Tet2*⁺/⁻, *Tet2*⁻/⁻, and *Tet2/3* double-deficient colonies re-plated from P4 to P5. Data shown are the means + SEM of 4 experiments for each genotype, assayed in triplicate.

(E and F) DNA dot-blot for 5hmC in primary mouse cKit⁺ cells cultured for 6 days ± L-ascorbic acid (L-AA) (E), and relative *Tet1*, *Tet2*, and *Tet3* mRNA levels in cKit⁺ cells, quantified by RT-PCR and normalized to *Hprt* (F). Data are representative of 2 experiments.

(G) Time course showing increase in 5hmC levels (quantified by flow cytometry) in peripheral blood cells of mice treated with a single i.p. injection of sodium ascorbate.

(H–J) Vitamin C treatment of mice reconstituted with *Tet2*⁺/⁺ and *Tet2*⁻/⁻ bone marrow. Mice were injected i.p. with PBS (control) or ascorbate (ASC, 4 g/kg), and white blood cell (WBC) counts were monitored for 24 weeks post-transplant (PT) (H). Frequency (I) and number (J) of donor B and T lymphocytes and myeloid cells (M) in peripheral blood of recipients at 24 weeks PT treated with ASC or control (PBS). *p < 0.05, **p < 0.005, and ***p < 0.005 in all experiments.

See also Figure S5.
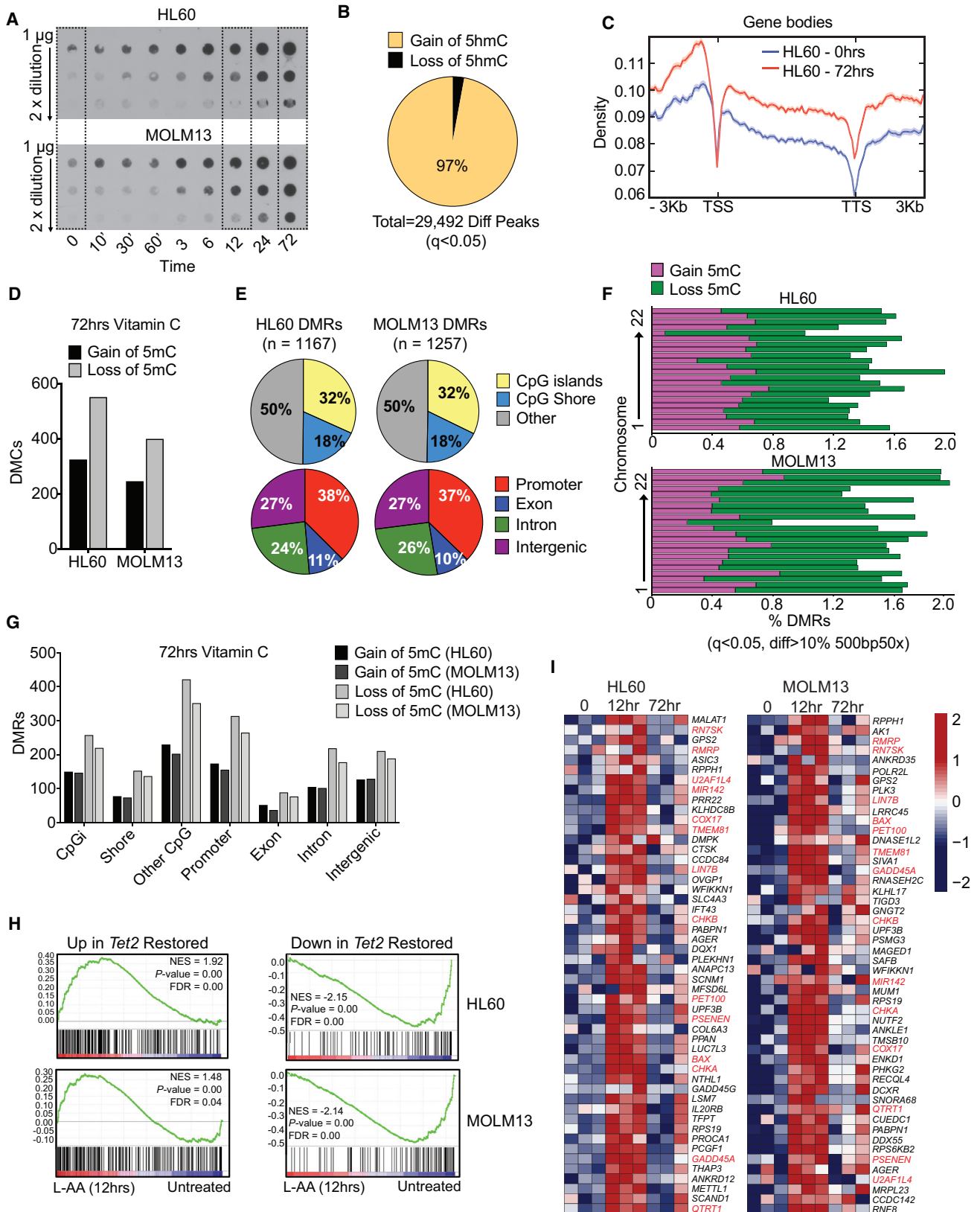
inhibitor olaparib and vitamin C (L-AA), at varying doses. Remarkably, combination olaparib/vitamin C treatment caused a greater loss in viability of HL60, MOLM13, THP1, and KG1 cells than either agent alone (Figures 7G and S7I).

DISCUSSION

We have found that targeted restoration of *Tet2* is sufficient to block aberrant self-renewal of pre-leukemic stem cells. Similarly, vitamin C, by enhancing the activity of TET family dioxygenases, acts as a pharmacologic mimic of *Tet2* restoration. Moreover, genetic or pharmacological restoration of TET activity confers an emergent vulnerability in leukemia cells, rendering them more sensitive to PARP inhibitors. Together, these results suggest new therapeutic strategies for clonal hematopoiesis, MDS and AML.

In the 1970s, Cameron et al. (1979) first administered high-dose intravenous (i.v.) vitamin C, in parallel with oral supplementation, to treat solid tumors, and saw some clinical responses. Subsequent clinical trials failed to show any therapeutic benefit of high-dose vitamin C, but these failures might have been due to the intrinsically limited bioavailability of orally administered vitamin C (Padayatty and Levine, 2016). Intracellular vitamin C levels in humans vary from 1 mM in WBCs to 10 mM in brain cells. Yet, following oral administration of very high doses of vitamin C (>500 mg/day), maximal plasma concentrations do not exceed 150 μM, due to homeostatic downregulation of the sodium-dependent vitamin C transporter that regulates intestinal absorption (Young et al., 2015). By contrast, i.v. administration of vitamin C can yield plasma levels up to 100-fold higher than normal levels with minimal toxicity (Padayatty and Levine, 2016).

Several recent clinical trials report some clinical benefit of high-dose i.v. vitamin C treatment of solid tumors (Fritz et al., 2014), yet the underlying therapeutic mechanism has remained largely undefined. One study suggested that vitamin C decreases viability of human leukemia cell lines by promoting downregulation of *HIF1*α and the anti-apoptotic genes, *BCL2*, *BCL2L1*, and *MCL1* (Kawada et al., 2013). Others recently showed that vitamin C selectively kills *KRAS* and *BRAF* mutant colorectal cancer cells by targeting *GAPDH* (Yun et al., 2015). Vitamin C treatment of various cancer cell lines also enhances the viral mimicry response to DNA methyltransferase inhibitors

such as 5-azacytidine (Liu et al., 2016). Given the diversity of α-KG and Fe^{2+}-dependent enzymes that utilize vitamin C as a co-factor (including prolyl-hydroxylases, jumonji histone deme-thylases, and TET enzymes) (Young et al., 2015), the mechanistic basis for vitamin C action could well depend on the type of cancer and/or its dependence on specific dioxygenases.

Most leukemia patients with *TET2* mutations or deletions exhibit mono-allelic *TET2* loss (Abdel-Wahab et al., 2009; Delhommeau et al., 2009), and disease progression in *Tet2*$^{+/-}$ and *Tet2*$^{-/-}$ mice is almost indistinguishable (Moran-Crusio et al., 2011), indicating that even a 50% loss of TET2 function can initiate aberrant hematopoiesis. We have found that vitamin C impairs aberrant re-plating capacity and myeloid disease progression in HSPCs even in the complete absence of functional *Tet2*. Recent studies have shown that *Tet2* and *Tet3* exhibit overlapping tumor suppressive roles, as both are highly expressed in myeloid progenitors and their combined deletion leads to rapid and aggressive AML (An et al., 2015). TET3 activation might compensate sufficiently for lack of TET2 to diminish aberrant self-renewal upon vitamin C treatment. Indeed, we find that combined *Tet2*/*Tet3* deficiency causes severe depletion of steady-state 5hmC in HSPC DNA, diminished capacity for 5hmC generation in response to vitamin C, and markedly decreased efficacy of vitamin C in suppressing aberrant self-renewal. These findings suggest that vitamin C acts predominantly through TETs, and accordingly, a minimal amount of TET activity is required for vitamin C action.

MDS and AML patients are typically elderly, with a median age of 65–70 years at disease onset. Intensive myeloablative treatment regimens are possible in only a minority of such patients and are associated with decreased efficacy and increased therapy-related mortality (Zeidan et al., 2014). DNA hypomethylating agents (HMAs) elicit higher overall response rates in MDS and AML patients with *TET2* mutations and provide an alternative to aggressive chemotherapy (Bejar et al., 2014). Re-expression of tumor suppressors has been the main focus of HMAs; however, the DNA damage response is also an important regulator of active DNA demethylation. While 5mC and 5hmC are stable modifications in the genome, 5fC and 5caC are normally present at very low levels, and their accumulation would lead to an increased requirement for BER to remove these modifications. This requirement, in turn, confers an emergent vulnerability on

Figure 6. Vitamin C Treatment Increases TET Activity in Human AML and Drives DNA Hypomethylation

(A) DNA dot blots for 5hmC in MOLM13 and HL60 cells treated for 72 hr with 250 μM L-ascorbic acid (L-AA). Data are representative of 2 experiments.

(B and C) Differentially hydroxymethylated peaks (Diff Peaks) with gain or loss of 5hmC (Diff Peaks, q < 0.05), assayed by 5hmeDIP-seq, in HL60 cells treated with 250 μM L-AA for 72 hr. Frequency and total number of significant Diff Peaks (B) and gene body distribution of the top 10,000 significant peaks following L-AA treatment (C), displayed as peak density ± 3 kb from the transcription start site (TSS) to the transcription termination site (TTS).

(D) Number of differentially methylated cytosines (DMCs), either hypermethylated (gain of 5mC) or hypomethylated (loss of 5mC), in HL60 and MOLM13 cells treated for 72 hr with 250 μM L-AA, assayed by bisulfite sequencing (q < 0.05, DiffMeth >25%).

(E–G) Differentially methylated regions (DMRs) in 72 hr L-AA-treated HL60 and MOLM13 cells (q < 0.05, DiffMeth >10%, 500 bp). Total DMR frequencies, according to CpG context and genomic location (E), are shown as the frequency of hypermethylated (gain of 5mC) or hypomethylated (loss of 5mC) DMRs across all chromosomes (F) and by the total number of DMRs with gain or loss of 5mC according to CpG context and genomic location (G).

(H) Gene-set enrichment analysis for up- and downregulated genes associated with 10 days of *Tet2* restoration in cKit$^+$ cells (497 upregulated and 136 downregulated, Log2FC, p < 0.05) in HL60 and MOLM13 cells treated with L-AA (250 μM) for 12 hr. Lowest gene expression (dark blue) to highest expression (red) is displayed for each plot.

(I) Heatmap showing expression of genes upregulated by *Tet2* restoration in cKit$^+$ cells in HL60 and MOLM13 cells treated with L-AA (250 μM) for 0, 12, or 72 hr. Scale represents log-transformed counts, normalized by library size, from lowest (dark blue) to highest expression (red). For all sequencing experiments, 3 replicates were analyzed per time point.

See also Figure S6.
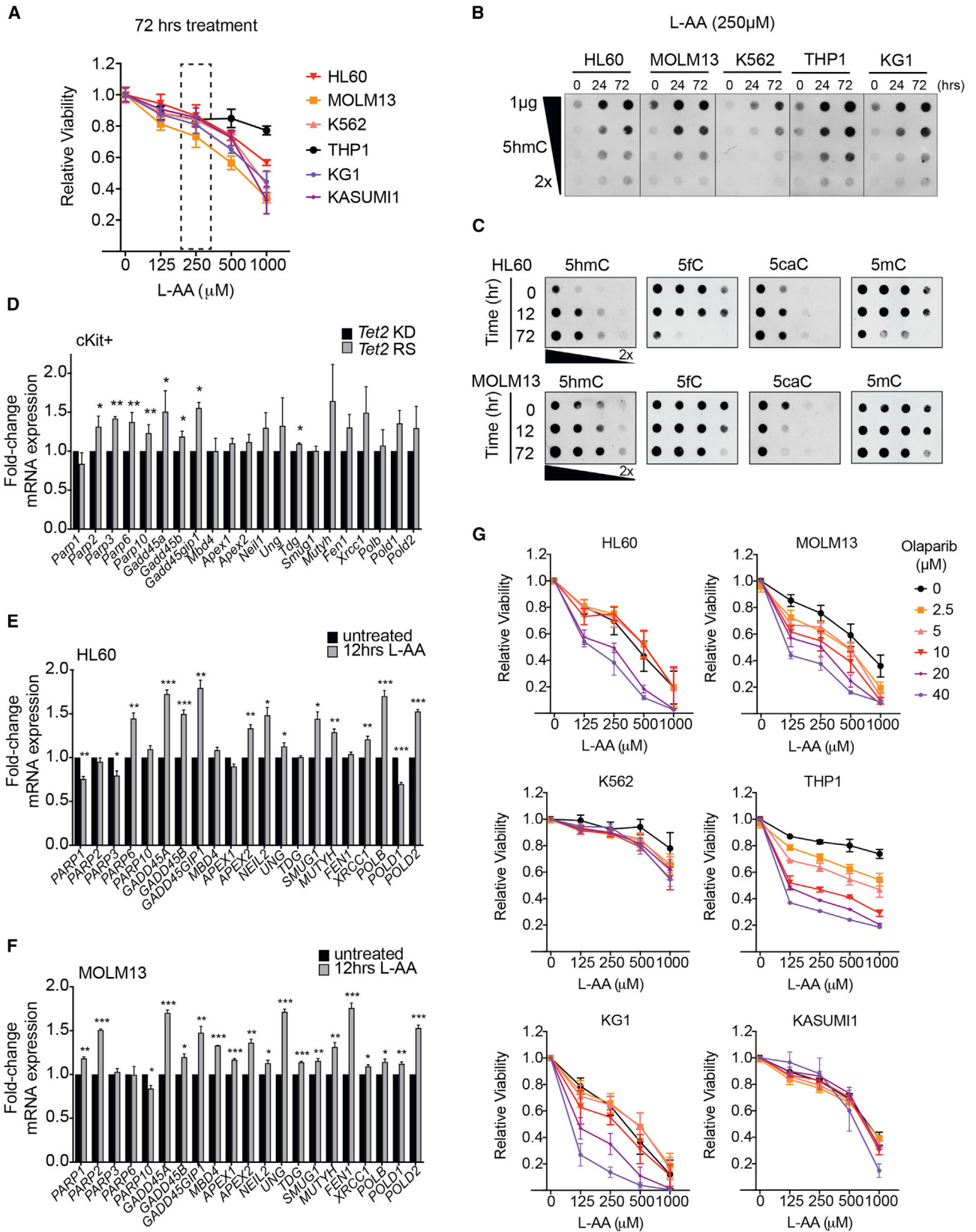
(legend on next page)

these cells, rendering them more sensitive to inhibitors of BER, such as PARPi, that can be exploited for targeted therapy.

Decreased TET expression and loss of 5hmC are seen in a wide variety of solid tumors, as well as in many hematologic malignancies (Rasmussen and Helin, 2016). Our results suggest that future clinical trials should incorporate high-dose vitamin C as an adjuvant to standard chemotherapy/demethylating therapy, especially for *TET2*-deficient neoplasms, and also predict further improvement in efficacy with the addition of PARP inhibition.

STAR★METHODS

Detailed methods are provided in the online version of this paper and include the following:

- KEY RESOURCES TABLE
- CONTACT FOR REAGENT AND RESOURCE SHARING
- EXPERIMENTAL MODEL AND SUBJECT DETAILS
  - ○ In vivo animal studies
  - ○ Primary cell culture
  - ○ Cell lines
  - ○ Patient samples
  - ○ Primary AML colony formation and liquid differentiation assays
  - ○ Xenotransplantation
- METHOD DETAILS
  - ○ Immunohistochemistry and microscopy
  - ○ Flow cytometry
  - ○ Bone marrow competitive transplantation
  - ○ Retroviral transduction
  - ○ Cell viability and cell cycle
  - ○ Quantitative RNA expression assays
  - ○ RNA sequencing analysis
  - ○ Gene set enrichment analysis
  - ○ Global DNA methylation quantitation
  - ○ Bisulfite sequencing
  - ○ Bisulfite sequencing analysis
  - ○ 5-hydroxymethylcytosine DNA immunoprecipitation (5hmeDIP), sequencing and analysis
- QUANTIFICATION AND STATISTICAL ANALYSIS
- DATA SOFTWARE AND AVAILABILITY

SUPPLEMENTAL INFORMATION

Supplemental Information includes seven figures and eight tables and can be found with this article online at http://dx.doi.org/10.1016/j.cell.2017.07.032.

An audio PaperClip is available at http://dx.doi.org/10.1016/j.cell.2017.07.032#mmc2.

REFERENCES

Abdel-Wahab, O., Mullally, A., Hedvat, C., Garcia-Manero, G., Patel, J., Wadleigh, M., Malinge, S., Yao, J., Kilpivaara, O., Bhat, R., et al. (2009). Genetic characterization of TET1, TET2, and TET3 alterations in myeloid malignancies. Blood *114*, 144–147.

Akalin, A., Kormaksson, M., Li, S., Garrett-Bakelman, F.E., Figueroa, M.E., Melnick, A., and Mason, C.E. (2012). methylKit: a comprehensive R package for the analysis of genome-wide DNA methylation profiles. Genome Biol. *13*, R87.

An, J., González-Avalos, E., Chawla, A., Jeong, M., López-Moyado, I.F., Li, W., Goodell, M.A., Chavez, L., Ko, M., and Rao, A. (2015). Acute loss of

---

Figure 7. TET-Mediated Oxidation of DNA in Vitamin C-Treated Leukemia Cells Increases Killing in Combination with PARP Inhibition

(A) Relative viability of human leukemia lines grown for 3 days in increasing concentrations of L-ascorbic acid (L-AA). Shown are means ± SD. Data for 4 experiments.

(B and C) Dot blots of genomic DNA from human leukemia lines subjected to 0, 24, and 72 hr of L-AA treatment, probed for 5hmC (B), and from HL60 and MOLM13 probed for 5hmC, 5fC, 5caC, and 5mC (C). Data are representative of 3 experiments.

(D–F) Fold-changes in mRNA levels of genes associated with BER and active DNA demethylation in *Tet2*-restored mouse HSPCs and vitamin C-treated human leukemia cells. Fold-changes were calculated from normalized counts from RNA-sequencing in day 10-restored cKit$^+$ cells, relative to knockdown (D), and in 12 hr L-AA-treated, relative to untreated, HL60 (E) and MOLM13 cells (F). *p < 0.05, **p < 0.00, and ***p < 0.005.

(G) Relative viability of AML lines treated with L-AA in combination with PARP inhibitor (Olaparib) at the indicated concentrations. Cells were assayed in triplicate at each concentration. Mean ± SEM are shown for 3 independent experiments.

See also Figure S7.

TET function results in aggressive myeloid cancer in mice. Nat. Commun. 6, 10071.

Barretina, J., Caponigro, G., Stransky, N., Venkatesan, K., Margolin, A.A., Kim, S., Wilson, C.J., Lehár, J., Kryukov, G.V., Sonkin, D., et al. (2012). The Cancer Cell Line Encyclopedia enables predictive modelling of anticancer drug sensitivity. Nature 483, 603–607.

Barreto, G., Schäfer, A., Marhold, J., Stach, D., Swaminathan, S.K., Handa, V., Döderlein, G., Maltry, N., Wu, W., Lyko, F., and Niehrs, C. (2007). Gadd45a promotes epigenetic gene activation by repair-mediated DNA demethylation. Nature 445, 671–675.

Bejar, R., Lord, A., Stevenson, K., Bar-Natan, M., Pérez-Ladaga, A., Zaneveld, J., Wang, H., Caughey, B., Stojanov, P., Getz, G., et al. (2014). TET2 mutations predict response to hypomethylating agents in myelodysplastic syndrome patients. Blood 124, 2705–2712.

Blaschke, K., Ebata, K.T., Karimi, M.M., Zepeda-Martínez, J.A., Goyal, P., Mahapatra, S., Tam, A., Laird, D.J., Hirst, M., Rao, A., et al. (2013). Vitamin C induces Tet-dependent DNA demethylation and a blastocyst-like state in ES cells. Nature 500, 222–226.

Booth, M.J., Ost, T.W., Beraldi, D., Bell, N.M., Branco, M.R., Reik, W., and Balasubramanian, S. (2013). Oxidative bisulfite sequencing of 5-methylcytosine and 5-hydroxymethylcytosine. Nat. Protoc. 8, 1841–1851.

Cadet, J., and Wagner, J.R. (2013). DNA base damage by reactive oxygen species, oxidizing agents, and UV radiation. Cold Spring Harb. Perspect. Biol. 5 http://dx.doi.org/10.1101/cshperspect.a012559.

Cameron, E., Pauling, L., and Leibovitz, B. (1979). Ascorbic acid and cancer: a review. Cancer Res. 39, 663–681.

Chen, J., Guo, L., Zhang, L., Wu, H., Yang, J., Liu, H., Wang, X., Hu, X., Gu, T., Zhou, Z., et al. (2013). Vitamin C modulates TET1 function during somatic cell reprogramming. Nat. Genet. 45, 1504–1509.

Chung, T.L., Brena, R.M., Kolle, G., Grimmond, S.M., Berman, B.P., Laird, P.W., Pera, M.F., and Wolvetang, E.J. (2010). Vitamin C promotes widespread yet specific DNA demethylation of the epigenome in human embryonic stem cells. Stem Cells 28, 1848–1855.

Ciccarone, F., Klinger, F.G., Catizone, A., Calabrese, R., Zampieri, M., Bacalini, M.G., De Felici, M., and Caiafa, P. (2012). Poly(ADP-ribosyl)ation acts in the DNA demethylation of mouse primordial germ cells also with DNA damage-independent roles. PLoS ONE 7, e46927.

Delhommeau, F., Dupont, S., Della Valle, V., James, C., Trannoy, S., Massé, A., Kosmider, O., Le Couedic, J.P., Robert, F., Alberdi, A., et al. (2009). Mutation in TET2 in myeloid cancers. N. Engl. J. Med. 360, 2289–2301.

Dow, L.E., Nasr, Z., Saborowski, M., Ebbesen, S.H., Manchado, E., Tasdemir, N., Lee, T., Pelletier, J., and Lowe, S.W. (2014). Conditional reverse tet-transactivator mouse strains for the efficient induction of TRE-regulated transgenes in mice. PLoS ONE 9, e95236.

Du, J., Cullen, J.J., and Buettner, G.R. (2012). Ascorbic acid: chemistry, biology and the treatment of cancer. Biochim. Biophys. Acta 1826, 443–457.

Esteban, M.A., Wang, T., Qin, B., Yang, J., Qin, D., Cai, J., Li, W., Weng, Z., Chen, J., Ni, S., et al. (2010). Vitamin C enhances the generation of mouse and human induced pluripotent stem cells. Cell Stem Cell 6, 71–79.

Figueroa, M.E., Lugthart, S., Li, Y., Erpelinck-Verschueren, C., Deng, X., Christos, P.J., Schifano, E., Booth, J., van Putten, W., Skrabanek, L., et al. (2010). DNA methylation signatures identify biologically distinct subtypes in acute myeloid leukemia. Cancer Cell 17, 13–27.

Fritz, H., Flower, G., Weeks, L., Cooley, K., Callachan, M., McGowan, J., Skidmore, B., Kirchner, L., and Seely, D. (2014). Intravenous vitamin C and cancer: a systematic review. Integr. Cancer Ther. 13, 280–300.

Gu, H., Smith, Z.D., Bock, C., Boyle, P., Gnirke, A., and Meissner, A. (2011). Preparation of reduced representation bisulfite sequencing libraries for genome-scale DNA methylation profiling. Nat. Protoc. 6, 468–481.

Guillamot, M., Cimmino, L., and Aifantis, I. (2016). The impact of DNA methylation in hematopoietic malignancies. Trends Cancer 2, 70–83.

Hochedlinger, K., Yamada, Y., Beard, C., and Jaenisch, R. (2005). Ectopic expression of Oct-4 blocks progenitor-cell differentiation and causes dysplasia in epithelial tissues. Cell 121, 465–477.

Kallin, E.M., Rodríguez-Ubreva, J., Christensen, J., Cimmino, L., Aifantis, I., Helin, K., Ballestar, E., and Graf, T. (2012). Tet2 facilitates the derepression of myeloid target genes during CEBPα-induced transdifferentiation of pre-B cells. Mol. Cell 48, 266–276.

Kawada, H., Kaneko, M., Sawanobori, M., Uno, T., Matsuzawa, H., Nakamura, Y., Matsushita, H., and Ando, K. (2013). High concentrations of L-ascorbic acid specifically inhibit the growth of human leukemic cells via downregulation of HIF-1α transcription. PLoS ONE 8, e62717.

Kim, W.I., Wiesner, S.M., and Largaespada, D.A. (2007). Vav promoter-tTA conditional transgene expression system for hematopoietic cells drives high level expression in developing B and T cells. Exp. Hematol. 35, 1231–1239.

Kosmider, O., Gelsi-Boyer, V., Ciudad, M., Racoeur, C., Jooste, V., Vey, N., Quesnel, B., Fenaux, P., Bastie, J.N., Beyne-Rauzy, O., et al.; Groupe Francophone des Myélodysplasies (2009). TET2 gene mutation is a frequent and adverse event in chronic myelomonocytic leukemia. Haematologica 94, 1676–1681.

Liu, M., Ohtani, H., Zhou, W., Ørskov, A.D., Charlet, J., Zhang, Y.W., Shen, H., Baylin, S.B., Liang, G., Grønbæk, K., and Jones, P.A. (2016). Vitamin C increases viral mimicry induced by 5-aza-2′-deoxycytidine. Proc. Natl. Acad. Sci. USA 113, 10238–10244.

Morales, J., Li, L., Fattah, F.J., Dong, Y., Bey, E.A., Patel, M., Gao, J., and Boothman, D.A. (2014). Review of poly (ADP-ribose) polymerase (PARP) mechanisms of action and rationale for targeting in cancer and other diseases. Crit. Rev. Eukaryot. Gene Expr. 24, 15–28.

Moran-Crusio, K., Reavie, L., Shih, A., Abdel-Wahab, O., Ndiaye-Lobry, D., Lobry, C., Figueroa, M.E., Vasanthakumar, A., Patel, J., Zhao, X., et al. (2011). Tet2 loss leads to increased hematopoietic stem cell self-renewal and myeloid transformation. Cancer Cell 20, 11–24.

Padayatty, S.J., and Levine, M. (2016). Vitamin C: the known and the unknown and Goldilocks. Oral Dis. 22, 463–493.

Pan, F., Wingo, T.S., Zhao, Z., Gao, R., Makishima, H., Qu, G., Lin, L., Yu, M., Ortega, J.R., Wang, J., et al. (2017). Tet2 loss leads to hypermutagenicity in haematopoietic stem/progenitor cells. Nat. Commun. 8, 15102.

Papaemmanuil, E., Gerstung, M., Bullinger, L., Gaidzik, V.I., Paschka, P., Roberts, N.D., Potter, N.E., Heuser, M., Thol, F., Bolli, N., et al. (2016). Genomic classification and prognosis in acute myeloid leukemia. N. Engl. J. Med. 374, 2209–2221.

Pastor, W.A., Aravind, L., and Rao, A. (2013). TETonic shift: biological roles of TET proteins in DNA demethylation and transcription. Nat. Rev. Mol. Cell Biol. 14, 341–356.

Premsrirut, P.K., Dow, L.E., Kim, S.Y., Camiolo, M., Malone, C.D., Miething, C., Scuoppo, C., Zuber, J., Dickins, R.A., Kogan, S.C., et al. (2011). A rapid and scalable system for studying gene function in mice using conditional RNA interference. Cell 145, 145–158.

Quivoron, C., Couronné, L., Della Valle, V., Lopez, C.K., Plo, I., Wagner-Ballon, O., Do Cruzeiro, M., Delhommeau, F., Arnulf, B., Stern, M.H., et al. (2011). TET2 inactivation results in pleiotropic hematopoietic abnormalities in mouse and is a recurrent event during human lymphomagenesis. Cancer Cell 20, 25–38.

Rasmussen, K.D., and Helin, K. (2016). Role of TET enzymes in DNA methylation, development, and cancer. Genes Dev. 30, 733–750.

Rasmussen, K.D., Jia, G., Johansen, J.V., Pedersen, M.T., Rapin, N., Bagger, F.O., Porse, B.T., Bernard, O.A., Christensen, J., and Helin, K. (2015). Loss of TET2 in hematopoietic cells leads to DNA hypermethylation of active enhancers and induction of leukemogenesis. Genes Dev. 29, 910–922.

Shen, L., Song, C.X., He, C., and Zhang, Y. (2014). Mechanism and function of oxidative reversal of DNA and RNA methylation. Annu. Rev. Biochem. 83, 585–614.

Shih, A.H., Jiang, Y., Meydan, C., Shank, K., Pandey, S., Barreyro, L., Antony-Debre, I., Viale, A., Socci, N., Sun, Y., et al. (2015). Mutational cooperativity

linked to combinatorial epigenetic gain of function in acute myeloid leukemia. Cancer Cell *27*, 502–515.

Sperling, A.S., Gibson, C.J., and Ebert, B.L. (2017). The genetics of myelodysplastic syndrome: from clonal haematopoiesis to secondary leukaemia. Nat. Rev. Cancer *17*, 5–19.

Wiehle, L., Raddatz, G., Musch, T., Dawlaty, M.M., Jaenisch, R., Lyko, F., and Breiling, A. (2015). Tet1 and Tet2 protect DNA methylation canyons against hypermethylation. Mol. Cell. Biol. *36*, 452–461.

Wilson, A., Laurenti, E., Oser, G., van der Wath, R.C., Blanco-Bose, W., Jaworski, M., Offner, S., Dunant, C.F., Eshkind, L., Bockamp, E., et al. (2008). Hematopoietic stem cells reversibly switch from dormancy to self-renewal during homeostasis and repair. Cell *135*, 1118–1129.

Yin, R., Mao, S.Q., Zhao, B., Chong, Z., Yang, Y., Zhao, C., Zhang, D., Huang, H., Gao, J., Li, Z., et al. (2013). Ascorbic acid enhances Tet-mediated 5-methylcytosine oxidation and promotes DNA demethylation in mammals. J. Am. Chem. Soc. *135*, 10396–10403.

Young, J.I., Züchner, S., and Wang, G. (2015). Regulation of the epigenome by vitamin C. Annu. Rev. Nutr. *35*, 545–564.

Yun, J., Mullarky, E., Lu, C., Bosch, K.N., Kavalier, A., Rivera, K., Roper, J., Chio, I.I., Giannopoulou, E.G., Rago, C., et al. (2015). Vitamin C selectively kills KRAS and BRAF mutant colorectal cancer cells by targeting GAPDH. Science *350*, 1391–1396.

Zeidan, A.M., Kharfan-Dabaja, M.A., and Komrokji, R.S. (2014). Beyond hypomethylating agents failure in patients with myelodysplastic syndromes. Curr. Opin. Hematol. *21*, 123–130.

STAR★METHODS

KEY RESOURCES TABLE

REAGENT or RESOURCE	SOURCE	IDENTIFIER
Antibodies		
Rabbit polyclonal anti-5hmC	Active Motif	Cat# 39791
Rabbit polyclonal anti-5fC	Active Motif	Cat# 61223
Rabbit polyclonal anti-5caC	Active Motif	Cat# 61229
Mouse monoclonal anti-5mC	Zymo Research	Cat# ZRC180674
Goat anti-rabbit IgG AlexaFluor594	Life Technologies	Cat# A11012
anti-mouse CD45.1 PercP-Cy5.5 conjugated (A20)	eBioscience	45-0453-82
anti-mouse CD45.2 Biotinylated (104)	BioLegend	109804
anti-mouse B220 PECy7 conjugated (RA3-6B2)	BD Biosciences	552772
anti-mouse CD3 APC conjugated (145-2C11)	BioLegend	100312
anti-mouse CD11b/Mac1 APCCy7-conjugated (M1/70)	BioLegend	101226
anti-mouse Gr1/Ly6G/C APCCy7 conjugated (RB6-8C5)	BioLegend	108424
anti-mouse CD71 PE conjugated (RI7217)	BioLegend	113808
anti-mouse Ter119 PerCP-Cy5.5 conjugated (TER-119)	BioLegend	116228
anti-mouse CD4 APCCy7 conjugated (RM4-5)	BioLegend	100526
anti-mouse CD8 APCCy7 conjugated (53-6.7)	BioLegend	100714
anti-mouse cKit APCCy7 conjugated (2B8)	BioLegend	105826
anti-mouse CD34 eFluor660 conjugated (RAM34)	eBioscience	50-0341-82
anti-mouse FcR eFluor450 conjugated (93)	eBioscience	48-0161-82
anti-mouse Sca1 PECy7 conjugated (D7)	BioLegend	108114
anti-mouse CD150 PE conjugated (TC15-12F12.2)	BioLegend	115904
anti-mouse CD48 Pacific blue conjugated (HM48-1)	BioLegend	103418
anti-human CD45 BV510 conjugated (2D1)	BD Biosciences	659482
anti-human CD99 FITC conjugated (TÜ12)	BD Biosciences	561986
anti-human CD34 Pacific Blue conjugated (581)	BioLegend	343511
anti-human CD38 PECy7 conjugated (HIT2)	BD Biosciences	560677
anti-human CD14 BV421 conjugated (MPhiP9)	BD Biosciences	659450
Streptavidin conjugated Pacific Blue	Life Technologies	Cat#S11222
Donkey anti-rabbit IgG HRP	GE Healthcare	NA934
Sheep anti-mouse IgG HRP	GE Healthcare	NA931
Rabbit polyclonal anti-GFP	ThermoFisher	A-11122
Rabbit polyclonal anti-TurboGFP	ThermoFisher	PA5-22688
Chemicals, Peptides, and Recombinant Proteins		
Phospholipid-binding Protein, APC Annexin V	BD PharMingen	Cat# BDB550474
DAPI (4',6-Diamidino-2-Phenylindole, Dihydrochloride)	ThermoFisher	Cat# D1306
L-ascorbic acid	Sigma Aldrich	Cat# A4544
2-Phospho-L-ascorbic acid	Sigma Aldrich	Cat# 49752
Sodium ascorbate	Sigma Aldrich	Cat# A4034-500G
Catalase	Sigma Aldrich	Cat# 1345
CM-H2DCFDA (chloromethyl derivative of H_2 dichlorofluorescein diacetate)	ThermoFisher	Cat# C6827
Recombinant mouse IL-3	PeproTech	Cat# 213-13
Recombinant mouse IL-6	PeproTech	Cat# 216-16
Recombinant mouse SCF	PeproTech	Cat# 250-03

(*Continued on next page*)

Continued

REAGENT or RESOURCE	SOURCE	IDENTIFIER
Recombinant human SCF	PeproTech	Cat# 300-07
Recombinant human IL-3	PeproTech	Cat# 200-03
Recombinant human G-CSF	PeproTech	Cat# 300-23
Recombinant human FLT3-L	PeproTech	Cat# 300-19
Doxycycline Hyclate	MP Biomedicals	ICN19895501
Polybrene	Millipore	Cat# TR-1003-G
Olaparib (AZD2281, Ku-0059436)	Selleckchem.com	Cat# S1060
Doxycycline grain-based rodent diet (1g/kg)	Bio-Serv	Cat# 14-726-309
Critical Commercial Assays		
MethylFlash Methylated DNA Quantification Kit (Colorimetric)	Epigentek	Cat# P-1034
MethylFlash Hydroxymethylated DNA Quantification Kit (Colorimetric)	Epigentek	Cat# P-1030
NEXTflex RNA-Seq Kit	Bioo Scientific	Cat# 5129-02
NEBNext Multiplex Oligos for Illumina (Index Primers Set 1)	New England Biolabs	Cat# E7335S
NEBNext Multiplex Oligos for Illumina (Index Primers Set 2)	New England Biolabs	Cat# E7500S
TrueMethyl Seq Kit	Cambridge Epigenetix	Cat# TM-03-001
CellTiter-Glo luminescence viability assay	Promega	Cat# PAG7572
AnnexinV APC apoptosis detection kit	BD bioscience	Cat# BDB559763
Deposited Data		
Raw and analyzed data	This paper	GEO: GSE97442
TET2-ChIP-seq data	Pan et al., 2017	GEO: GSE74390
Human reference genome UCSC build hg19 (GRCh37)	Genome Reference Consortium	http://genome.ucsc.edu/cgi-bin/hgGateway?db=hg19
Mouse reference genome UCSC build mm10 (GRCm38)	Genome Reference Consortium	http://genome.ucsc.edu/cgi-bin/hgGateway?db=mm10
Human gene annotation	Ensembl	http://grch37.ensembl.org/Homo_sapiens/Info/Annotation
Mouse gene annotation	Ensembl	http://useast.ensembl.org/Mus_musculus/Info/Annotation
Experimental Models: Cell Lines		
Human: HL-60	ATCC	CCL-240
Human: MOLM-13	DSMZ	ACC 554
Human: KG-1	ATCC	CCL-246
Human: KASUMI-1	ATCC	CRL-2724
Human: THP-1	ATCC	TIB-202
Human: K562	ATCC	CCL-243
Human: PlatinumE	CELL BIOLABS	RV-101
Experimental Models: Organisms/Strains		
Mouse: Vav-tTA	Kim et al., 2007	N/A
Mouse: TRE-shRen	Dow et al., 2014	N/A
Mouse: B6.Cg-Gt(ROSA)26Sortm1(rtTA*M2)Jae/J (Rosa26-M2rtTA)	The Jackson Laboratory	Stock No: 006965
Mouse: B6.129-Flt3tm1Dgg/J (Flt3-ITD)	The Jackson Laboratory	Stock No: 011112
Mouse: TRE-shTet2	Mirimus / This paper	N/A
Mouse: TRE-shTet3	Mirimus / This paper	N/A
Mouse: B6.SJL-Ptprca Pepcb/BoyJ (CD45.1)	The Jackson Laboratory	Stock No: 002014
Mouse: NOD.Cg-Prkdcscid Il2rgtm1Wjl Tg(CMV-IL3,CSF2,KITLG)1Eav/MloySzJ (NSGS)	The Jackson Laboratory	Stock #013062
Mouse: B6.FVB-Tg(EIIa-cre)C5379Lmgd/J (E2a-Cre)	The Jackson Laboratory	Stock No: 003724

(*Continued on next page*)

Continued

REAGENT or RESOURCE	SOURCE	IDENTIFIER
Mouse: B6;129S-Tet2tm1.1Iaai/J (Tet2 floxed)	The Jackson Laboratory	Stock No. 017573
Oligonucleotides		
shRNA targeting sequence: mTet2: ATAGGACTATA ATGTATAGATA	Moran-Crusio et al., 2011	N/A
shRNA targeting sequence: Renilla luciferase: CAGGAATTATAATGCTTATCTA	Dow et al., 2014	N/A
shRNA targeting sequence: mTet3: CCCGGATTGAG AAGGTCATCTA	This paper	N/A
Genotyping primer: Rosa-M2rtTA mutant GCGAAGA GTTTGTCCTCAACC	Hochedlinger et al., 2005	N/A
Genotyping primer: Rosa26 common AAAGTCGCT CTGAGTTGTTAT	Hochedlinger et al., 2005	N/A
Genotyping primer: Rosa26 wild-type GGA GCG GGA GAA ATG GAT ATG	Hochedlinger et al., 2005	N/A
Genotyping primer: Vav-tTA Forward: CCATACTCA CTTTTGCCCTTTAG	Kim et al., 2007	N/A
Genotyping primer: Vav-tTA Reverse: CAGCGCGC TGAGTGCATATAATGCA	Kim et al., 2007	N/A
Genotyping primer: SADPA Reverse: ATCAAGGAA ACCCTGGACTACTGCG	Premsrirut et al., 2011	N/A
Genotyping primer: COLA1 Forward: AATCATCCC AGGTGCACAGCATTGCGG	Premsrirut et al., 2011	N/A
Genotyping primer: COLA1 Reverse: CTTTGAGGG CTCATGAACCTCCCAGG	Premsrirut et al., 2011	N/A
Genotyping primer: COLTGM Reverse: GAAAGAA CAATCAAGGGTCC	Premsrirut et al., 2011	N/A
Genotyping primer: TRE-shRen Forward: TAGATAA GCATTATAATTCCTATGCC	This paper	N/A
Genotyping primer: TRE-shTet2 Forward TATCTAT ACATTATAGTCCTAC	This paper	N/A
Genotyping primer: TRE-shTet3 Forward: TAGATG ACCTTCTCAATCCGGATGCC	This paper	N/A
qRT-PCR Primer: mTet2 Forward: AGAGCCTCAA GCAACCAAAA	This paper	N/A
qRT-PCR Primer: mTet2 Reverse: ACATCCCTGA GAGCTCTTGC	This paper	N/A
qRT-PCR Primer: mTet1 Forward: AGCTGGATTG AAGGAACAGG	This paper	N/A
qRT-PCR Primer: mTet1 Reverse: GTCTCCATGA GCTCCCTGAC	This paper	N/A
qRT-PCR Primer: mTet3 Forward: AGAGCCTCAAGCA	This paper	N/A
qRT-PCR Primer: mTet3 Reverse	This paper	N/A
qRT-PCR Primer: mHprt Forward: CAGTACAGCC CCAAAATGGT	This paper	N/A
qRT-PCR Primer: mHprt Reverse: CAAGGGCATA TCCAACAACA	This paper	N/A
qRT-PCR Primer: hTET2 Forward: CAGCACATTG GTATGCACTC	This paper	N/A
qRT-PCR Primer: hTET2 Reverse: TTTCCTTTGTC GGCAAGTCT	This paper	N/A
qRT-PCR Primer: hTET1 Forward: CAGCTGTCTT GATCGAGTTA	This paper	N/A

Continued

REAGENT or RESOURCE	SOURCE	IDENTIFIER
qRT-PCR Primer: hTET1 Reverse: AATTGGACA CCCATGAGAGC	This paper	N/A
qRT-PCR Primer: hTET3 Forward: CGATTGCGT CGAACAAATAG	This paper	N/A
qRT-PCR Primer: hTET3Reverse: CTCCTTCCCC GTGTAGATGA	This paper	N/A
qRT-PCR Primer: hGAPDH Forward: CTCCTCC TGTTCGACAGTCAGC	This paper	N/A
qRT-PCR Primer: hGAPDH Reverse: CCATGGAA TTTGCCATGGGTGG	This paper	N/A
Recombinant DNA		
Plasmid: AML-ETO9a-IRES-mCherry	This paper	N/A
Software and Algorithms		
STAR	N/A	https://github.com/alexdobin/STAR
featureCounts	N/A	http://subread.sourceforge.net/
DESeq2	N/A	https://bioconductor.org/packages/ release/bioc/html/DESeq2.html
Trim Galore!	N/A	https://www.bioinformatics.babraham. ac.uk/projects/trim_galore/
Bismark	N/A	https://www.bioinformatics.babraham. ac.uk/projects/bismark/
Bowtie2	N/A	http://bowtie-bio.sourceforge.net/bowtie2/
methylKit	Akalin et al., 2012	https://github.com/al2na/methylKit

CONTACT FOR REAGENT AND RESOURCE SHARING

Further information and requests for resources and reagents should be directed to and will be fulfilled by the Lead Contact, Iannis Aifantis (Ioannis.aifantis@nyumc.org).

EXPERIMENTAL MODEL AND SUBJECT DETAILS

In vivo animal studies

TRE-TurboGFP-shTet2, and *TRE-TurboGFP-shTet3* transgenic mice were generated by Mirimus by using previously described protocols (Premsrirut et al., 2011). *Vav-tTA*, *Rosa-M2rtTA* and *TRE-GFP-Ren* mice have been described previously (Dow et al., 2014; Hochedlinger et al., 2005; Kim et al., 2007). Doxycycline food (1g/kg) was administered to regulate shRNA expression *in vivo*. C57BL/6 (B6.SJL-*Ptprca Pepcb/BoyJ* (CD45.1) mice were purchased from Jackson Laboratory and bred in a mouse facility at NYU Medical Center. Germ-line *Tet2*-deficient mice have been described previously (Moran-Crusio et al., 2011). For bone marrow transplantation studies, sex-matched recipient mice of both sexes, aged 8-10 weeks, were transplanted with donor and support bone marrow cells isolated from mice aged 6-8 weeks.

Primary cell culture

Total bone marrow cells from *Vav-tTA or Flt3^{ITD};Rosa-rtTA shRen/shTet2*, *Tet2^{+/+}*, *Tet2^{+/−}* and *Tet2^{−/−}* mice (6-8 weeks) or purified bone marrow cKit+ cells from *Rosa-rtTA shRen/shTet2* mice transduced with *AE9a-IRES-mCherry* retrovirus were plated in methylcellulose medium (Methocult M3434 or M3534, Stem Cell Technologies). Cells were seeded at 20,000 total bone marrow cells or 2000 purified cKit+ cells per replicate. Colony forming units were enumerated using a Zeiss Axio Observer microscope and re-plated (2,000 cells/replicate) every 7–10 days. Primary mouse hematopoietic progenitor cells from *Vav-tTA shTet2, Rosa-M2rtTA shRen/shTet2* mice in combination with *Flt3^{ITD}* or *AE9a* were cultured in OpitMEM (GIBCO) with 10% FBS, 100 U/mL penicillin, 100 μg/ml streptomycin, 50 μM 2-mercaptoethanol and recombinant mouse SCF (50ng/ml), IL3 (10ng/ml) and IL6 (10ng/ml) at 37°C in 5% CO_2. Doxycycline (Dox) was used at a final concentration of 1 μg/ml for all cell culture assays. For vitamin C treatment, L-ascorbic acid (L-AA) or ascorbate (ASC) was added directly to methylcellulose or liquid culture medium at a final concentration of 250 μM unless otherwise indicated. Catalase treatment was performed at a concentration of 1unit/ml of medium.

Cell lines

The human leukemia lines HL60, MOLM13, K562, KG1, THP1 and KASUMI1 were grown in RPMI (GIBCO). PlatinumE cells used for retroviral transfections were maintained in DMEM with 10%–20% FBS. Media were supplemented wtih 100 U/mL penicillin, 100 μg/ml streptomycin and cultures were incubated at 37°C, 5% CO_2.

Patient samples

Diagnostic BM aspirates were obtained from AML patients treated at Memorial Sloan Kettering Cancer Center (MSKCC) or Princess Margaret Cancer Center (PMCC). All samples were collected after obtaining written informed consent. The use of human materials was approved by the Institutional Review Boards of MSKCC and Princess Margaret Cancer Center in accordance with the Helsinki Declaration.

Primary AML colony formation and liquid differentiation assays

Blasts (SSC^{low}, CD45^{int}, CD99^{high}) and residual HSPC (SSC^{low}, CD45^{int}, CD34$^+$, CD38$^-$, CD99^{low}) from primary AML specimens were double FACS–sorted to > 95% purity and seeded in methylcellulose (MethoCult H4435, Stem Cell Technologies). After 14 days, colonies were counted under an Olympus BX41 microscope. For liquid differentiation assays, sorted cells were plated at 1x10^6/mL in Stem Span (Stem Cell Technologies) media, supplemented with human cytokines that support monocyte/macrophage differentiation: SCF (50 ng/mL), IL-3 (10 ng/mL), Fms-like tyrosine kinase-3–ligand (FLT3-L; 50 ng/mL), G-CSF (10 ng/mL) (Peprotech). After 7 days, immunophenotypic analysis was performed by flow cytometry for CD14 expression.

Xenotransplantation

Experiments were carried out in accordance with institutional guidelines approved by MSKCC. NSGS (6-10 weeks-old) mice were bred under pathogen-free conditions. For xenotransplantation, mice were sub-lethally irradiated (200-250 cGy) 3-24 hr before transplantation by direct intrafemoral injection. CD34+ cells purified by immunomagnetic selection from viably frozen patient bone marrow or peripheral blood mononuclear cells (Miltenyi Biotec) were used as the source of cells for xenografts. CBC analysis was performed on peripheral blood collected from submandibular bleeding using a Procyte Dx Hematology Analyzer (IDEXX Veterinary Diagnostics).

METHOD DETAILS

Immunohistochemistry and microscopy

Tissues were dissected from mice for fixation overnight in 10% formalin (Fisher). Fixed tissues were dehydrated and embedded in paraffin for sectioning. Paraffin sections (5 μm) were prepared and stained with hematoxylin and eosin (H&E) (Leica Autostainer XL). For immunohistochemistry, GFP or TurboGFP antibodies (ThermoFisher) were used and counterstained with hematoxylin. Fluorescence imaging and light microscopy were performed by using a Zeiss Axio Observer microscope.

Flow cytometry

Single cell suspensions were prepared from bone marrow, spleen or peripheral blood. Red blood cells were lysed with ammonium-chloride-potassium (ACK) buffer, and the remaining cells were resuspended in PBS with 3% FBS. Non-specific antibody binding was blocked by incubation with 20 μg/ml Rat IgG (Sigma-Aldrich) for 15 min, and cells were then incubated with primary antibodies for 30 min on ice. For 5hmC detection, cells were fixed at room temperature with 3% paraformaldehyde, permeabilized with 0.2% Triton X-100, denatured with 2N HCl, neutralized with 100 mM Tris-HCl, pH 8.0, and incubated with anti-5hmC (1:400) or isotype control antibodies for 30 min. Cells were then washed with PBS, incubated with secondary antibodies conjugated to AlexaFluor 594 (1:500) for 30 min, washed again and resuspended in PBS for flow cytometry. For detection of ROS activity, the cell permeable cloromethyl-2′,7′-dichlorofluorescin diacetate (CM-H2DCFDA) reagent was used (0.3 μM for *Tet2*-deficient cells or 1 μM for human AML cell lines). Upon oxidation, CM-H2DCFDA is converted to 2′, 7′ -dichlorofluorescein (DCF), which is then detected by fluorescence spectroscopy (excitation/emission spectra of 495nm/529nm, respectively). Stained cells were quantified using a BD Fortessa analyzer or isolated with a MoFlo cell sorter (Beckman Coulter) or BD ARIA II. FlowJo software (TreeStar) was used to generate flow cytometry plots.

Bone marrow competitive transplantation

Freshly dissected femurs and tibiae were isolated from donor Vav-tTA, *Tet2*+/+ or *Tet2*−/− (CD45.2+), as well as *Tet2*+/+ (CD45.1+) mice. Bones were flushed with PBS using a 22.5 gauge needle, and the isolate was centrifuged (5 min, 0.5g, 4°C) and treated with red cell lysis buffer, as described above. Total nucleated bone marrow cells were re-suspended in PBS, passed through a 40 μM cell strainer and counted. Donor cells (0.5 × 10^6 per genotype, per mouse) were mixed 1:1 with support bone marrow cells (CD 45.1+), and transplanted via retro-orbital injection into lethally irradiated (2 × 550 Rad) CD45.1+ recipient mice. Chimerism was monitored by flow cytometry (anti-CD45.1 and anti-CD45.2, BD Bioscience) of peripheral blood at 4-week intervals post-transplant for 20 weeks, at which time mice were sacrificed and chimerism was assessed in other hematopoietic compartments (bone marrow and spleen).

Retroviral transduction

Hematopoietic stem and progenitor cells were isolated by sorting Lin−cKit+Sca1+ cells, cultured in the presence of 50 ng/ml SCF, 50 ng/ml Flt3 ligand, 10 ng/ml IL-3, and 10 ng/ml IL-6, and infected with concentrated supernatants of *AML-ETO9a-IRES-mCherry* retrovirus after 24 and 48 hr. Transduction efficiency was determined by reporter fluorescence at 96 hr, and 2,000 sorted cKit+ cells were plated in methylcellulose media (M3434) for colony formation assays, as described above.

Cell viability and cell cycle

Apoptosis assays were performed by staining with Annexin V (BD PharMingen) according to the manufacturer's instructions, in combination with DAPI. The CellTiter-Glo Luminescent Cell viability assay kit (Promega), which is based on luminescent quantification of ATP, was also used to assess relative viability of cell cultures. For cell cycle studies, cells were fixed in 4% paraformaldehyde, permeabilized in 0.2% saponin and stained with 2 μg/ml DAPI prior to flow cytometric analysis.

Quantitative RNA expression assays

Total RNA was extracted from cells using the RNeasy Plus Mini Kit (QIAGEN). RNA quantity and quality were determined by using an Agilent 2100 Bioanalyzer. RNA-seq libraries were prepared from total RNA by polyA selection using oligo-dT beads (Life Technologies), according to the manufacturer's instructions. The resulting poly A+ RNA served as input for library construction using standard Illumina protocols. Sequencing was performed on an Illumina HiSeq 2500 sequencer using 50 bp single reads. For mRNA quantification, total RNA was used for cDNA synthesis using Superscript III first strand synthesis kit (Invitrogen). Real-time PCR reactions were carried out using SYBR Green Master Mix (Roche) and a Lightcycler 480 II (Roche).

RNA sequencing analysis

Sequencing results were demultiplexed and converted to FASTQ format by using Illumina bcl2fastq software. Sequencing reads were aligned to the human or mouse genomes, as appropriate (build hg19/GRCh37 and mm10/GRCm38, respectively), by using the splice-aware STAR aligner [https://www.ncbi.nlm.nih.gov/pubmed/23104886]. The featureCounts program [https://www.ncbi.nlm.nih.gov/pubmed/24227677] was utilized to generate counts for each gene based on how many aligned reads overlapped its exons. For sequencing depth and alignment results summary see Tables S4 and S5. Counts were then normalized and used to test for differential expression by using negative binomial generalized linear models, as implemented by the DESeq2 R package [https://www.ncbi.nlm.nih.gov/pubmed/25516281].

Gene set enrichment analysis

Gene set enrichment analysis was performed using gene set as permutation type, 1,000 permutations and log2 ratio of classes, or with gene set and Signal2Noise as metrics for ranking genes. Gene sets used in this study were identified from the Molecular Signatures Database (MSigDB Curated v4.0). Gene pathways and functions were assessed using Ingenuity Pathway Analysis (QIAGEN Bioinformatics).

Global DNA methylation quantitation

DNA samples were isolated by proteinase K digestion and phenol/chloroform extraction. DNA was denatured, and 2-fold serial dilutions were spotted on a nitrocellulose membrane in an assembled Bio-Dot apparatus (Bio-Rad). The blotted membrane was washed, air-dried, baked for 2hrs, blocked with 5% TBS-T, and incubated with rabbit polyclonal anti-5hmC, anti-5fC, or anti-5caC antibodies or mouse monoclonal anti-5mC antibody (1:1000) and HRP-conjugated anti-rabbit or anti-mouse IgG secondary antibodies (1:3000). ELISAs for 5hmC and 5mC were performed using MethylFlash hydroxymethylated and methylated DNA quantification kits (colorimetric, Epigentek), according to the manufacturer's instructions.

Bisulfite sequencing

Genomic DNA (gDNA) was isolated from mouse HSPCs and human AML cells grown in vitro. DNA methylation sequencing was performed and analyzed using reduced representation bisulphite sequencing (RRBS) methodology, as described previously (Gu et al., 2011). Oxidative bisulfite treatment was performed by using a TruMethyl-Seq Kit (CEGX) to generate oxRRBS libraries. The amplified libraries were sequenced on an Illumina HiSeq2500 with 50 bp single-end reads, following standard Illumina sequencing protocols. Primary and downstream data analyses, including calculation of differential methylation, were performed using Methylkit (Akalin et al., 2012).

Bisulfite sequencing analysis

Sequencing results were demultiplexed and converted to FASTQ format using Illumina bcl2fastq software. The sequencing reads were quality- and adaptor-trimmed using Trim Galore [https://www.bioinformatics.babraham.ac.uk/projects/trim_galore/] in RRBS mode. The trimmed reads were aligned to the human or mouse genomes (build hg19/GRCh37 and mm10/GRCm38, respectively), as appropriate, by using Bismark [https://www.ncbi.nlm.nih.gov/pubmed/21493656] with Bowtie 2 aligner [https://www.ncbi.nlm.nih.gov/pubmed/22388286]. Bismark also was used for methylation calls. Differential methylation analysis and annotation was performed with the methylKit R package [https://www.ncbi.nlm.nih.gov/pubmed/23034086]. For tiling windows analysis, the

genome was divided into 500 bp windows, and methylation information was summarized for each tile. Regions with low coverage (below 50X) or very high coverage (above 99.9th percentile) were discarded (for sequencing depth and alignment results summary see Tables S6 and S7).

5-hydroxymethylcytosine DNA immunoprecipitation (5hmeDIP), sequencing and analysis

Genomic DNA (0.5 μg) isolated from HL60 human AML cells was sonicated using a Covaris sonicator followed by end-repair, A-tailing and adaptor ligation using standard Illumina protocols. Ten percent (10%) of the input volume was retained prior to immunoprecipitation with anti-5hmC antibodies (1 μg/ml, Active Motif) at 4°C overnight. Immunoprecipitated DNA was recovered on protein G magnetic beads (Invitrogen), and DNA was purified from input and immunoprecipitated samples using Ampure beads, after proteinase K digestion followed by PCR amplification of libraries.

Libraries were sequenced on an Illumina HiSeq 2500 sequencer. Sequencing results were demultiplexed and converted to FASTQ format by using Illumina bcl2fastq. Reads were aligned to the human genome (build hg19/GRCh37) with Bowtie 2 [https://www.ncbi.nlm.nih.gov/pubmed/22388286] using local alignment. Only confidently mapped reads (mapping quality > 30) were retained. Duplicate reads were discarded using Picard [http://broadinstitute.github.io/picard/]. MACS [https://www.ncbi.nlm.nih.gov/pubmed/18798982] was utilized to perform peak calling with a q-value cutoff of 0.05. The R Bioconductor package DiffBind [https://bioconductor.org/packages/release/bioc/html/DiffBind.html] was used for identifying sites that are differentially bound between sample groups. The differential analysis method was set to use the DESeq2 package for more conservative full library size normalization and to avoid the assumption that most of the sites are not differentially bound. Profile plots of enrichment at genomic intervals were generated using deepTools [https://www.ncbi.nlm.nih.gov/pubmed/24799436]. Sequencing depth and alignment results are summarized in Table S8.

QUANTIFICATION AND STATISTICAL ANALYSIS

All p values were calculated using unpaired two-tailed Student's t test with Graphpad Prism software, unless otherwise described in the methods or figure legends. No specific randomization or blinding protocol was used for these analyses. Statistically significant differences are indicated with asterisks in figures with the accompanying p value in the legend. Error bars in figures indicate standard deviation (SD) or standard error of the mean (SEM) for the number of replicates, as indicated in the figure legend.

DATA SOFTWARE AND AVAILABILITY

The accession number for the raw and analyzed data of RNA-sequencing, Bisulfite-sequencing and 5-hydroxymethylcytosine DNA immunoprecipitation experiments performed in mouse cells and human cell lines reported in this paper is GEO: GSE97442.

A

6 months

20 months

GFP+ Cell Frequency (%)

E
M
T
B

B

% Overall survival

VTA shRen (n=21)
VTA shTet2 (n=16)

P = 0.0038

Time (day)

C

Spleen weight (g)

VTA shRen   *VTA shTet2*

D

VTA shRen   *VTA shTet2*

E

VTA shRen   *VTA shTet2*

Spleen

GFP

H&E

F

VTA shRen   *VTA shTet2*

Liver

GFP

H&E

Scale bar = 100μM

G

VTA shRen   *VTA shTet2*

cKit / Lin

0.294   10.5

Gr1 / CD11b

7.33   31.9

CD71 / Ter119

0.0905   2.5
4.95   34.1

H

VTA shRen   *VTA shTet2*

cKit / Sca-1

7.23   2.5
17.3   9.16

FcR / CD34

29.5
62.4   0.579
60
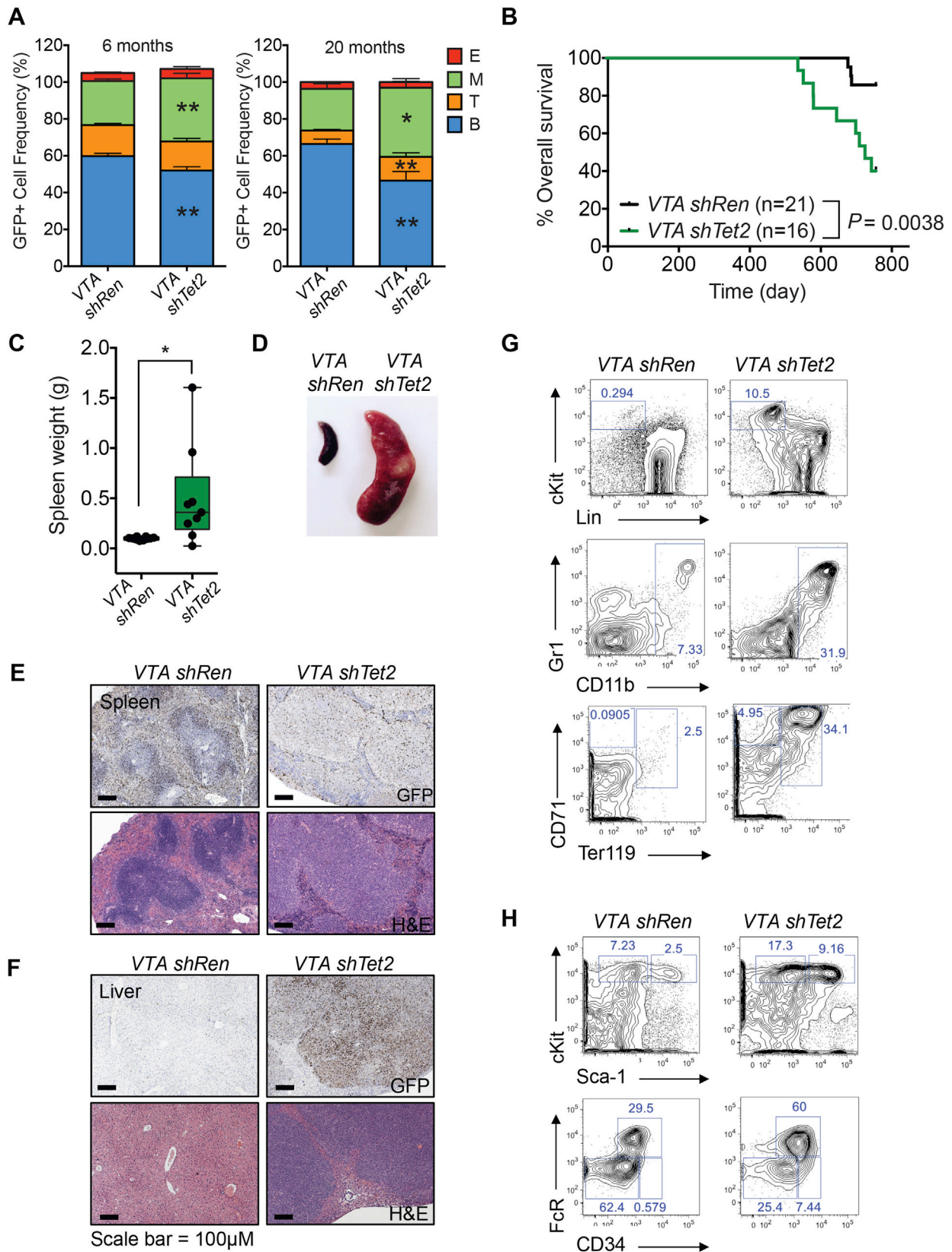25.4   7.44

(legend on next page)

Figure S1. *Tet2* Knockdown Mice Show Aberrant Stem Cell Phenotypes and Develop Myelo-erythroid Neoplasms, Related to Figure 1

(A) Cohorts of *Vav-tTA* (*VTA*) *shRen* (n = 16) and *VTA shTet2* mice (n = 21) were aged for 2 years in the absence of Dox treatment. Peripheral blood cell (PBC) lineages were monitored by flow cytometry at 6 months and 20 months. Cells were stained for B220 (B cells), CD3 (T cells) CD11b and Gr1 (Myeloid cells) and CD71 and Ter119 (erythroid cells). B, T, M, and E cell frequencies, respectively, were measured in GFP+ (shRNA)-expressing cells (70%–90% of PBCs). Stacked bars represent mean + SEM, *p < 0.05, **p < 0.005.

(B) Kaplan-Meier curve of untreated *VTA shRen* and *VTA shTet2* mice.

(C) Spleen weights of sick *VTA shTet2* mice compared with age-matched control *VTA shRen* mice. Floating bars show the mean ± SD (n = 9 mice per genotype), *p < 0.05.

(D) Image of representative spleens from sick *VTA shTet2* mice, compared with age-matched control *VTA shRen* mice.

(E and F) Histological analysis showing GFP/hematoxylin staining (upper panels) and H&E staining (lower panels) of spleen (E) and liver (F) sections from age-matched control *VTA shRen* and sick *VTA shTet2* mice. Scale bar = 100 μm in all panels. Data are representative of 9 mice per genotype.

(G and H) Representative flow cytometric analysis of control *VTA shRen* and sick *VTA shTet2* mouse spleen cells. Staining is shown for cKit+ progenitors versus lineage-positive cells, Gr1 versus CD11b+ myeloid cells and CD71 versus Ter119+ erythroid cells, all gated on GFP+ (shRNA-expressing) cells (H) GFP+ bone marrow cells were stained for Lineage-Sca1+cKit+cell HSPC (upper panel). FcR and CD34 staining (lower panel) to quantify myeloid-erythroid progenitor (MEP), common-myeloid progenitor (CMP) and granulocyte and myeloid-progenitor (GMP) cell frequency. Data are representative of 5 mice per genotype.
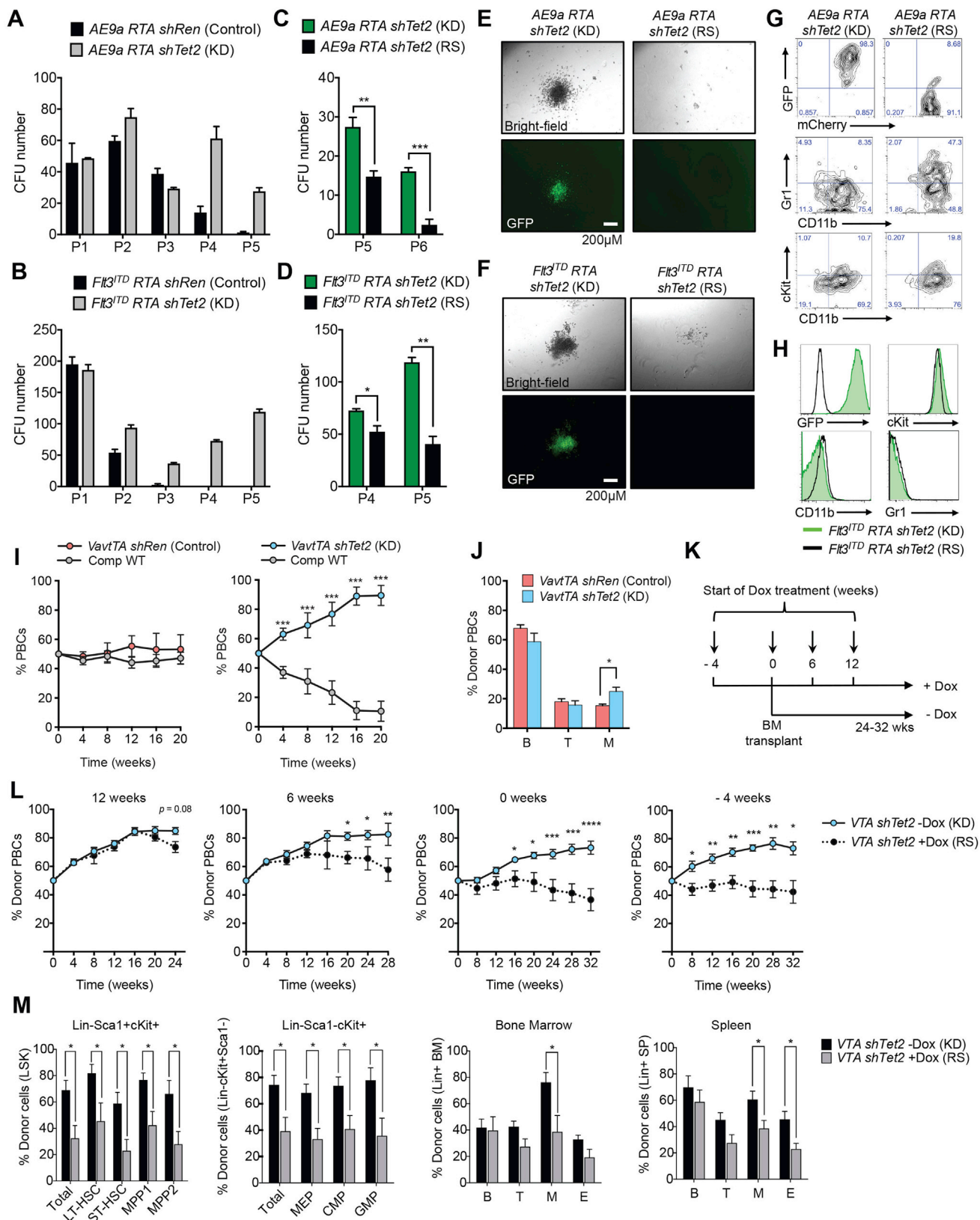
Figure S2. *Tet2* Restoration Suppresses In Vitro Replating Capacity and Corrects HSC Aberrant Self-Renewal In Vivo, Related to Figure 2

(A) Total cKit+ *Rosa-M2rtTA (RTA) shRen* or *RTA shTet2* cells transduced with *AML-ETO9a-IRES-mCherry* (AE9aC) virus after sort purification 2 days post-transduction were plated in methylcellulose media (M3434, Stem Cell Technologies) containing Dox (1 μg/ml) to maintain knockdown of *Tet2*. Cells (2,000/well, assayed in triplicate) were re-plated 5 times (P1-P5) every 7-10 days, and colony forming units (CFU) were enumerated at each plating. Data are representative of 2 experiments.

(B) *Flt3^ITD^;Rosa-M2rtTA (RTA) shRen* or *Flt3^ITD^; RTA shTet2* cells were plated in methylcellulose media (M3534, Stem Cell Technologies) containing Dox (1 μg/ml) to maintain knockdown of *Tet2*. Cells (2,000/well, assayed in triplicate) were re-plated every 7-10 days and colony-forming units (CFU) were quantified at each re-plating (P2-P5). Data are representative of 2 experiments.

(C) *AE9aC RTA shTet2* colony cells from P4 were re-plated ± Dox (1 μg/ml) for 2 additional platings. CFUs from *AE9a RTA shTet2* cells treated with Dox to maintain knockdown (KD) were compared to those with restoration (RS) of endogenous *Tet2* expression following Dox withdrawal. Colony forming assays were performed in triplicate. Data are representative of 2 experiments.

(D) *Flt3^ITD^; RTA shTet2* cells from P3 colonies were re-plated ± Dox (1 μg/ml) for 2 additional platings. CFUs from *Flt3^ITD^; RTA shTet2* cells treated with Dox to maintain knockdown (KD) were compared to those from cells in which endogenous *Tet2* expression was restored by Dox withdrawal. Colony forming assays were performed in triplicate. Data are representative of 2 experiments.

(E and F) Representative microscopy of colonies generated by *shTet2* knockdown (KD) or restored (RS) cultures from *AE9aC RTA shTet2* at plating 6 (P6) (E) and *Flt3^ITD^; RTA shTet2* at plating 5 (P5) (F).

(G and H) Representative flow cytometric analysis of *shTet2* knockdown (KD) or restored (RS) cells. *AE9aC RTA shTet2* colonies analyzed for GFP versus mCherry expression (upper panels). Note loss of GFP expression upon Dox withdrawal in AE9aC mCherry+ cells. Cells were also stained for Gr1/CD11b (middle panels) and cKit/CD11b (lower panels) (G). *Flt3^ITD^; RTA shTet2* KD or RS colonies showing loss of GFP expression upon Dox withdrawal, as well as surface expression of cKit, CD11b and Gr1 (H).

(I and J) Frequency of donor peripheral blood cells (PBCs) in bone marrow from mice reconstituted with donor *VTA shRen* control or *VTA shTet2* donor bone marrow cells (*Tet2* knockdown) and competitor WT bone marrow. The frequency of donor PBCs was measured over 20 weeks (I), and the frequencies of donor B, T and myeloid cells, M, were quantified at 20 weeks post-transplant (J). Data are presented as means ± SEM, n = 6 mice per genotype and are representative of 2 experiments.

(K) Schematic representation of in vivo experiments to test treatment with Dox food (1g/kg) to restore *Tet2* expression 4 weeks prior to competitive BM transplantation (−4 weeks), on the day of transplant (0 weeks), or 6 or 12 weeks post-transplant.

(L) Donor peripheral blood cell (PBC) frequency in reconstituted mice with donor *VTA shTet2* donor bone marrow cells (mean ± SEM, n = 4-5 mice per group).

(M) Frequency of donor bone marrow and spleen cells in mice sacrificed after treatment ± Dox food from 6-28 weeks post-transplant. Long-term (LT)-HSC (CD150^+^CD48^−^), short-term (ST)-HSC (CD150^−^CD48^−^), multipotent progenitor (MPP)-1 (CD150^+^CD48^+^) and MPP-2 (CD150^−^CD48^+^) donor chimerism are shown in addition to CMP, MEP and GMP myeloid progenitors and lineage-positive cells. (Mean ± SEM, n = 4-5 mice per group). *p < 0.05, **p < 0.005, ***p < 0.0005.
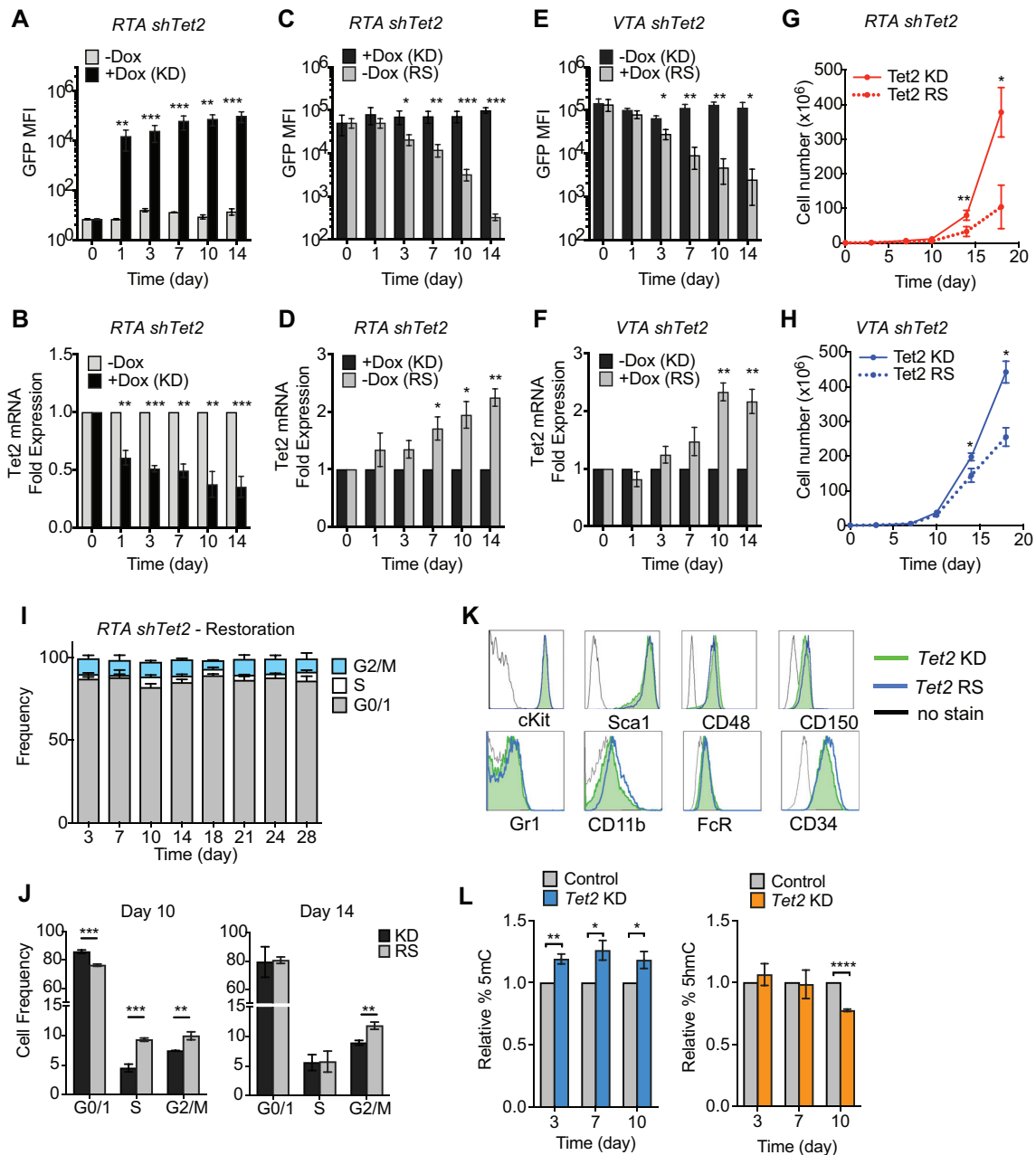
Figure S3. *Tet2* Restoration Promotes Differentiation and Induces Cell Death, Related to Figure 3

(A–F) In vitro culture of *Tet2* inducible and reversible knockdown cKit+ progenitor cells. Total cKit+ cells were purified and maintained in media containing SCF, IL3 and IL6. *RTA shTet2* cells were left untreated (DMSO) or treated with Dox (1ug/ml) to induce *Tet2* knockdown (KD). Mean fluorescence intensity (MFI) of GFP was assessed by flow cytometry (A) and expression of *Tet2* mRNA was quantified by qRT-PCR (B). *RTA shTet2* cKit+ cells grown for 4 weeks in the presence of Dox were subjected to Dox withdrawal over a 14-day period to restore *Tet2* expression (RS) or maintained in Dox (KD). MFI of GFP was assessed by flow cytometry (C) and expression of *Tet2* mRNA was quantified by q-RT-PCR (D). *Vav-tTA shTet2* ckit+ cells grown for 4 weeks in the absence of Dox were treated with Dox for 14 days (RS) or left untreated (KD). MFI of GFP expression was assessed by flow cytometry (E), and expression of *Tet2* mRNA (F) was quantified by q-RT-PCR. All *Tet2* mRNA expression data were normalized to *Hprt*. Data are shown as mean ± SD, and are representative of 4 experiments with 2 biological replicates per genotype, assayed in triplicate. *p < 0.05, **p < 0.005, ***p < 0.0005.

(G and H) Total cell number in cultures of *RTA shTet2* (G) and *VTA shTet2* cKit+ cells (H) with 18 days of sustained *Tet2* knockdown (KD) or *Tet2* restoration (RS), as indicated. Data are representative of 2 experiments with 2 biological replicates per genotype, assayed in triplicate. Mean ± SEM, *p < 0.05, **p < 0.005.

(I and J) Cell-cycle analysis of cultured *RTA shTet2* cKit+ cells. The frequencies of cells in G0/1, S and G2/M after 28 days of *Tet2* restoration (I), and at days 10 and 14 of *Tet2* restoration (RS), were compared to knockdown (KD) cells (J). Data are shown as mean ± SEM, and are representative of 2 experiments., *p < 0.05, **p < 0.005 and ***p < 0.0005.

(legend continued on next page)

(K) Representative flow cytometric analysis of stem and progenitor (cKit, Sca-1, CD48, CD150 and CD34) or differentiation (Gr1, CD11b and FcR) markers upon *Tet2* knockdown (KD) or restoration (RS) after 21 days of culture.

(L) Global changes in methylation were assessed in genomic DNA isolated from *RTA shTet2* cKit+ cells during inducible *Tet2* knockdown (KD) upon treatment with 1ug/ml DOX, compared with DNA from control, untreated cells. Quantification was performed using ELISAs for 5-methylcytosine (5mC) and 5-hydroxymethylcytosine (5hmC), respectively. Data are shown as mean $\pm$ SEM from 3 biological replicates, performed in triplicate *$p < 0.05$, **$p < 0.005$ and ***$p < 0.005$.
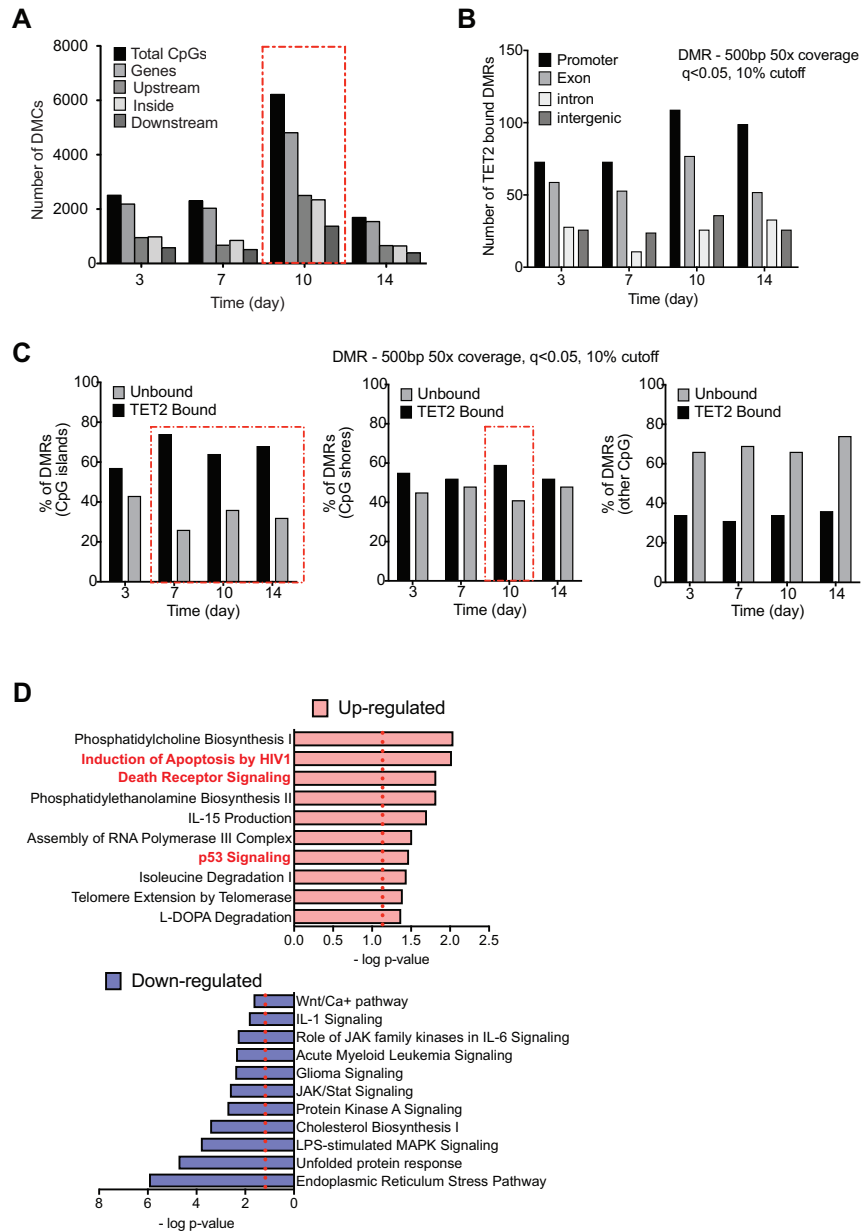
Figure S4. *Tet2* Restoration Leads to Changes in DNA Methylation and Gene Expression, Related to Figure 4

(A) Number of differentially methylated cytosines (q < 0.05, differential methylation > 10%) in total CpGs and in the indicated genomic regions of cKit + cells subjected to 14 days of *Tet2* restoration in vitro.

(B and C) Genomic context of TET2-bound differentially methylated regions (DMRs). The number of TET2-bound DMRs according to genomic location (B) and the frequency of TET2 bound and unbound DMRs according to CpG context (C) are shown.

(D) Ingenuity pathway analysis of canonical pathways involving up and downregulated genes following 10 days of *Tet2* restoration.
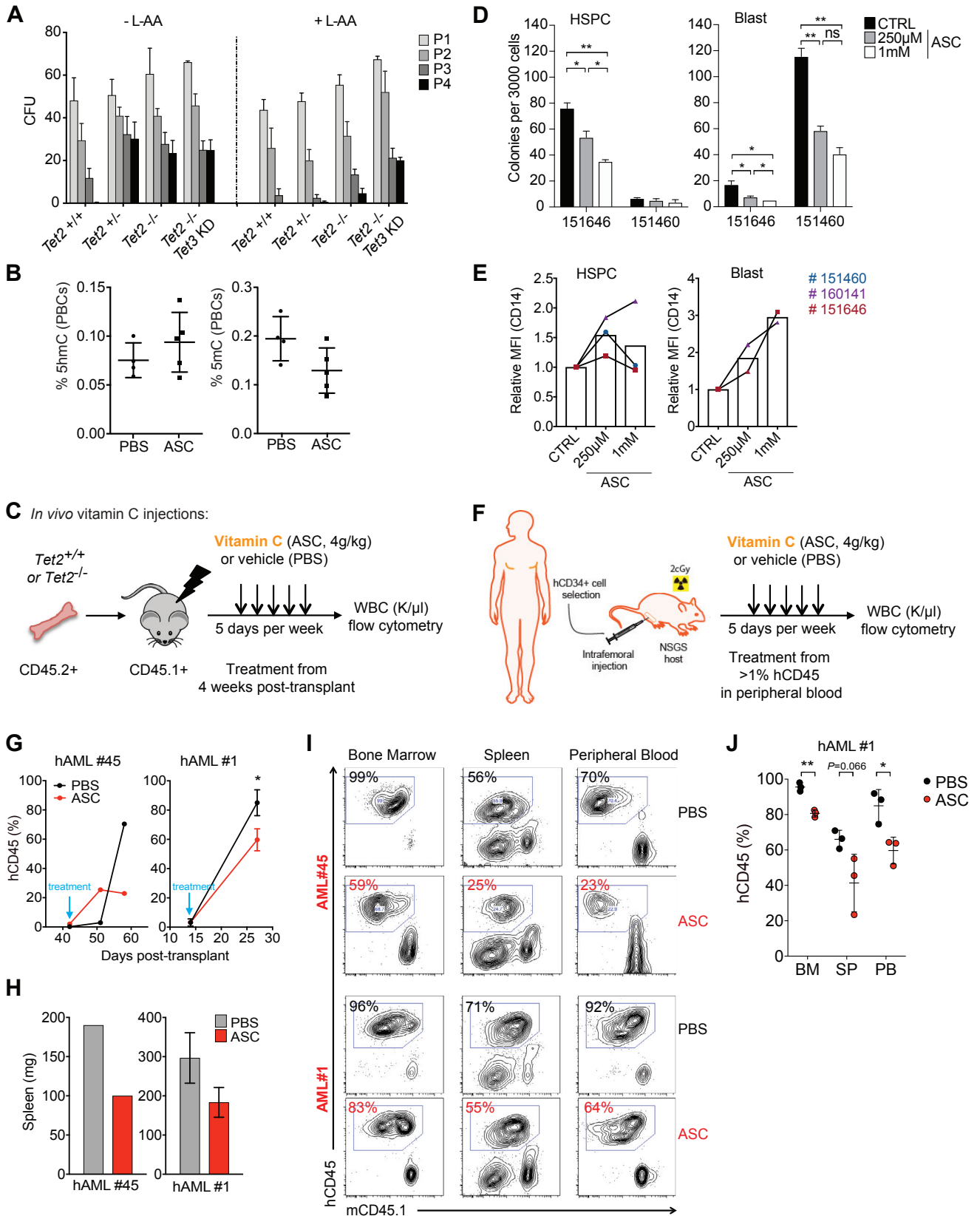
A - L-AA / + L-AA

CFU; P1, P2, P3, P4; Tet2 +/+, Tet2 +/-, Tet2 -/-, Tet2 -/- Tet3 KD

B % 5hmC (PBCs); % 5mC (PBCs); PBS, ASC

C *In vivo* vitamin C injections:

Tet2+/+ or Tet2−/−; CD45.2+; CD45.1+

Vitamin C (ASC, 4g/kg) or vehicle (PBS); 5 days per week; WBC (K/µl) flow cytometry; Treatment from 4 weeks post-transplant

D HSPC; Blast; Colonies per 3000 cells; CTRL, 250µM ASC, 1mM ASC; 151646, 151460

E HSPC; Blast; Relative MFI (CD14); # 151460, # 160141, # 151646; CTRL, 250µM, 1mM, ASC

F hCD34+ cell selection; 2cGy; Intrafemoral injection; NSGS host; Vitamin C (ASC, 4g/kg) or vehicle (PBS); 5 days per week; WBC (K/µl) flow cytometry; Treatment from >1% hCD45 in peripheral blood

G hAML #45; hAML #1; hCD45 (%); PBS, ASC; treatment; Days post-transplant

H Spleen (mg); PBS, ASC; hAML #45, hAML #1

I Bone Marrow; Spleen; Peripheral Blood; AML#45; AML#1; PBS, ASC; 99%, 56%, 70%, 59%, 25%, 23%, 96%, 71%, 92%, 83%, 55%, 64%; hCD45; mCD45.1

J hAML #1; hCD45 (%); PBS, ASC; BM, SP, PB; P=0.066

(legend on next page)

Figure S5. Vitamin C Treatment Corrects Aberrant Self-Renewal In Vitro and Controls Disease Progression in AML Xenograft Models, Related to Figure 5

(A) Colony formation assays with *Tet2* $^{+/+}$, *Tet2* $^{+/-}$, *Tet2* $^{-/-}$ and *Tet2* $^{-/-}$*Tet3*^{KD} bone marrow cells treated with L-AA (250 μM). Colonies were enumerated at four successive passages (P1-P4). Data are presented as mean CFU + SD from assays performed in triplicate and are representative of 4 experiments.

(B) The percentages of 5hmC and 5mC in total DNA, measured by ELISA, in peripheral blood cells (PBCs) of mice treated daily for 3 days with vehicle (PBS) or vitamin C (ASC, 4g/kg) injected IP (n = 4-5 mice per group).

(C) Schematic representation of vitamin C treatment experiments. Bone marrow from CD45.2^{+} *Tet2*$^{+/+}$ or *Tet2*$^{-/-}$ mice was transplanted into lethally irradiated CD45.1^{+} recipients, and treatment with vehicle (PBS) or vitamin C (ASC) was administered for 5 days per week beginning at 4 weeks post-transplant. Disease progression was monitored by blood counts and flow cytometry.

(D and E) Colony formation and liquid differentiation assays of primary AML patient samples treated with ascorbate (ASC) or left untreated. HSPCs (SSC^{low}, CD45^{int}, CD34^{+}, CD38^{-}, CD99^{low}) and blasts (SSC^{low}, CD45^{int}, CD99^{high}) were purified from primary AML specimens (#151646, #151460 and #160141) and seeded in methylcellulose (MethoCult H4435, Stem Cell Technologies) or grown in liquid culture with SCF, IL3, G-CSF or FLT3-L. Colony forming units (CFU) were quantified after 14 days (D), and cells grown in liquid culture were assayed after 7 days by flow cytometric analysis of CD14 levels (E). Note that sample #160141 did not give rise to colonies under either condition, although it did proliferate in liquid culture. Data are shown as mean ± SD of assays performed in triplicate in a single experiment.

(F) Schematic representation of primary human AML PDX generation and vitamin C treatment. Sub-lethally irradiated NSGS mice were transplanted with purified CD34+ cells from primary human AML samples by intrafemoral injection. Vehicle (PBS) or vitamin C (ASC) was administered by IP injection 5 days per week beginning after detection of hCD45+ cells (> 1%) in the peripheral blood of recipient mice. Disease progression was monitored by blood counting and flow cytometry.

(G–J) Disease progression in AML PDXs treated with vitamin C (ASC) or vehicle (PBS) was monitored by flow cytometric analysis of hCD45+ cells in peripheral blood (G). Upon sacrifice, spleen weight was measured (H) and the frequency of donor hCD45.2+ cells versus mCD45.1 recipient cells was quantified by flow cytometry in bone marrow (BM) spleen (SP) and peripheral blood (PB). Representative flow plots (I) and the frequency (mean ± SD) of hCD45+ cells (J) are shown. Two independent primary human AML specimens were tested: AML#1 (n = 3 per group) and AML#45 (n = 1 per group)., *p < 0.05, **p < 0.005 (Also see Table S2).
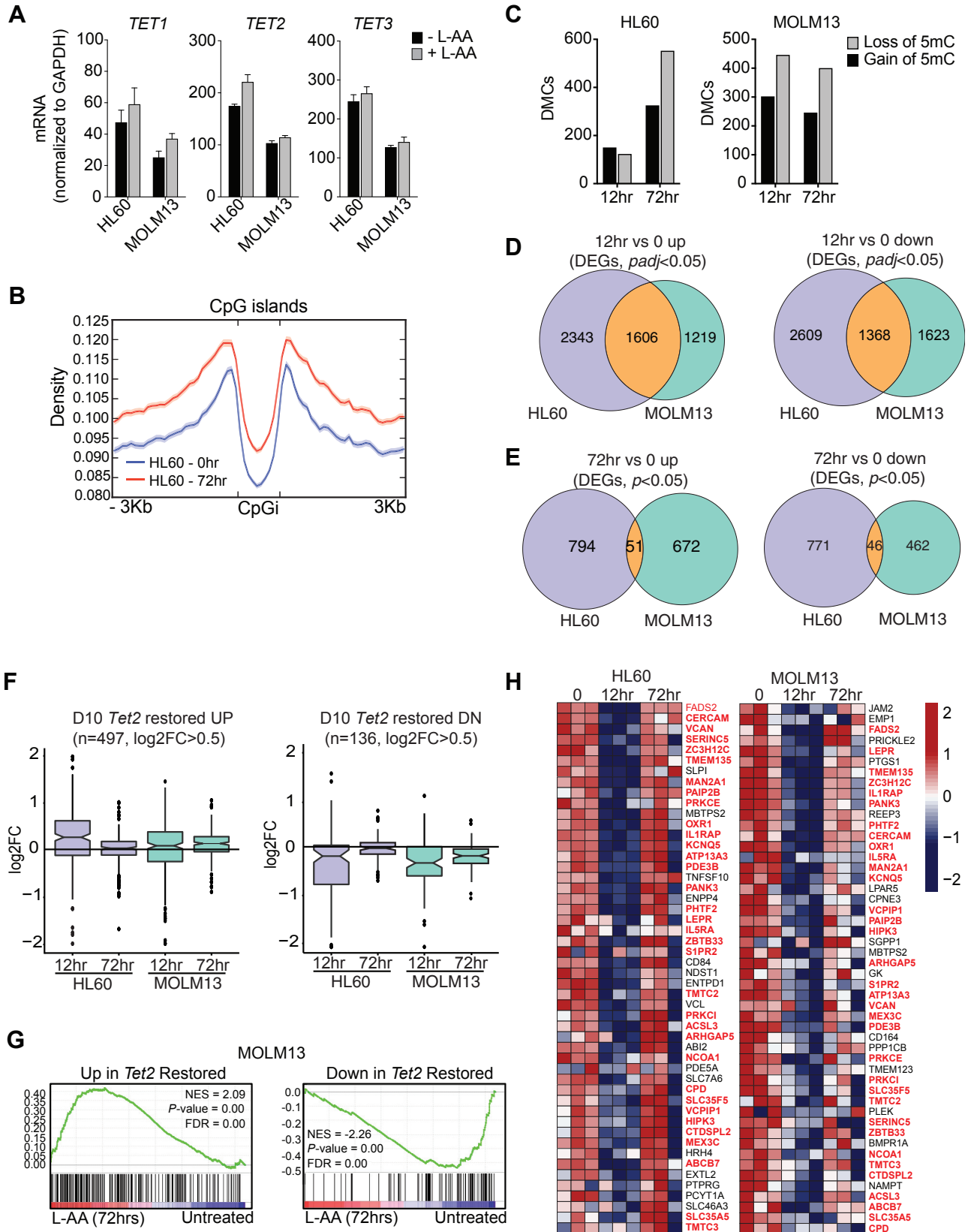
(legend on next page)

Figure S6. Vitamin C Treatment Alters 5mC, 5hmC, and Gene Expression Landscapes Mimicking In Vitro *Tet2* Restoration, Related to Figure 6

(A) TET mRNA levels (assessed by qRT-PCR) in the human leukemia cell lines HL60 and MOLM13 treated for 3 days with L-AA (250 μM) or left untreated. Data (mean ± SEM) are representative of 3 experiments.

(B) Peak density of 5hmC across CpG islands and shores (±3Kb) in untreated (0 hr) or L-AA treated (250 μM, 72hrs) HL60 cells, as assayed by 5hmeDIP-seq (q < 0.05).

(C) Number of differentially methylated cytosines (DMCs) hypermethylated or hypomethylated in HL60 and MOLM13 cells treated for 12 and 72hrs with 250 μM L-AA, as assessed by bisulfite sequencing (q < 0.05, Differential Methylation > 25%).

(D and E) Venn diagrams of RNA-sequencing analysis, displaying gene expression changes (*padj* < 0.05) in HL60 and MOLM13 treated with 250 μM L-AA for 12hrs (C) and 72hrs (D).

(F) Log2 fold-changes in gene signatures generated from *Tet2*-restored (day 10 of restoration) cKit+ cells (497 upregulated and 136 downregulated, p < 0.05) in HL60 and MOLM13 cells treated for 12 and 72hrs with 250 μM L-AA.

(G) Gene-set enrichment analysis of *Tet2*-restored genes in MOLM13 cells treated for 72hrs with 250 μM L-AA. Lowest gene expression (dark blue) to highest expression (red) is displayed for each GSEA plot.

(H) Heat-maps of *Tet2*-restored, downregulated gene signatures in HL60 and MOLM13 cells treated with 250 μM L-AA for 0, 12 and 72hrs. Heat-map scale represents log-transformed counts normalized with respect to library size from lowest (dark blue) to highest expression (red).
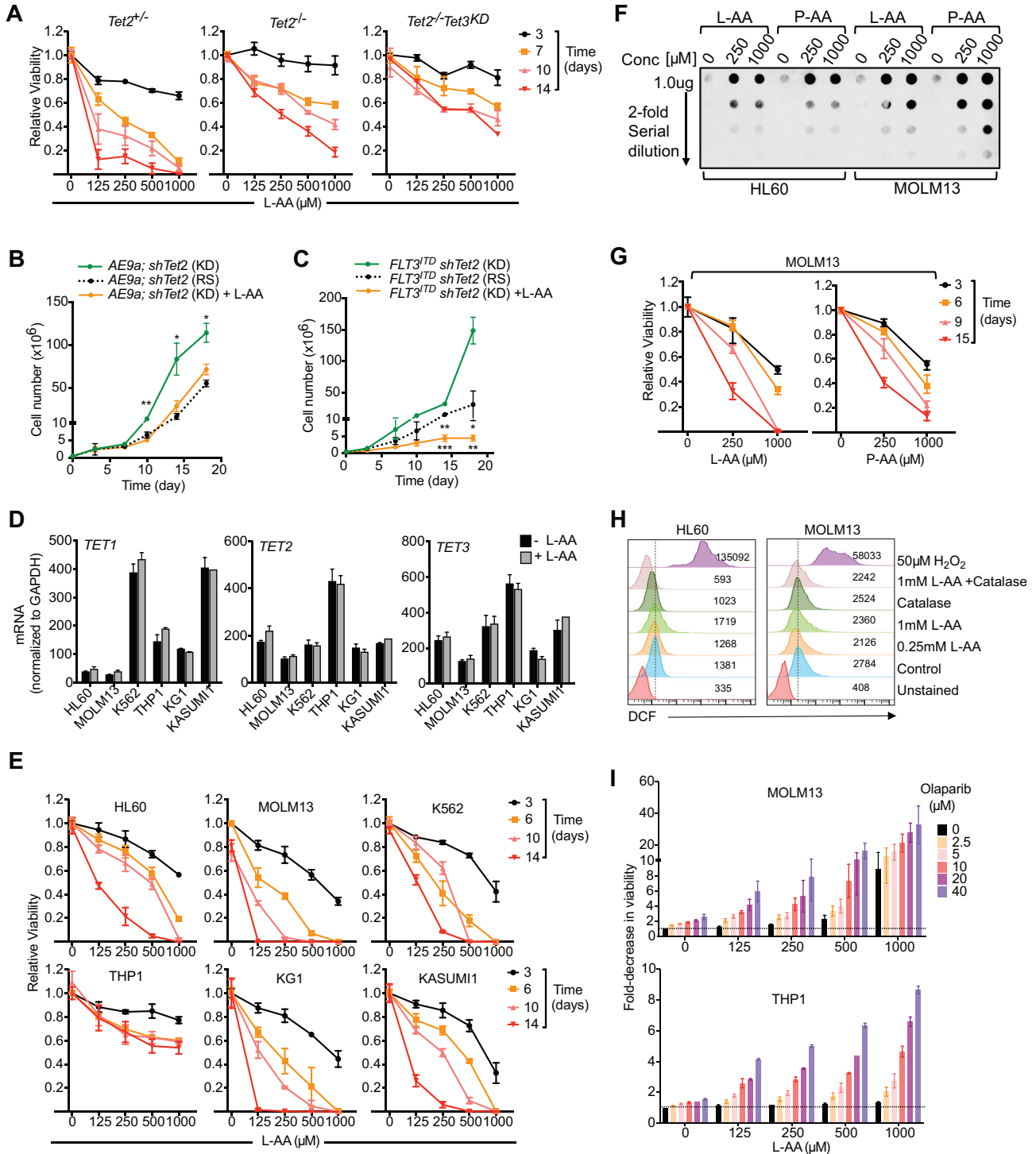
Figure S7. Effects of Vitamin C and PARPi Treatment on Human AML Cell Growth and Mouse Progenitors Expressing AML Oncogenes, Related to Figure 7

(A) Viability of $Tet2^{+/-}$ $Tet2^{-/-}$ and $Tet2^{-/-}Tet3^{KD}$ cell lines maintained for up to 14 days in increasing concentrations of L-ascorbic acid (L-AA), as indicated. Data (mean ± SD) are representative of 2-3 biological replicates and 2 experiments.

(B and C) Total number of $AE9a; RTA$ $shTet2$ (B) or $Flt3^{ITD}$ RTA $shTet2$ cKit+ (C) cells exposed to sustained $Tet2$ knockdown (KD), $Tet2$ restoration (RS) or $Tet2$ knockdown in combination with 250 μM L-AA. Data (mean ± SEM) are representative of 2 experiments with 2 biological replicates per genotype, assayed in triplicate, *p < 0.05, **p < 0.005.

(legend continued on next page)

(D) *TET* mRNA levels (by q-RT-PCR) in human leukemia cell lines treated for 3 days ± L-AA. Data (mean ± SEM) are representative of 3 experiments.

(E) Viability of human myeloid leukemia cell lines maintained for 14 days in increasing concentrations of L-ascorbic acid (L-AA). Data (mean ± SD) are representative of 2 experiments.

(F and G) HL60 and MOLM13 cells were treated for 72 hr with 0, 250 μM and 1000 μM L-AA or 2-phospho-L-ascorbic acid (P-AA). 5hmC levels (F) were assessed by dot blot and cell proliferation was quantified over 2 weeks of treatment (G). Data (mean ± SD) are representative of 2 experiments.

(H) Intracellular ROS in HL60 and MOLM13 cells was quantified by DCF fluorescence following treatment with L-AA ± Catalase for 3 hr. Untreated (CTL) and hydrogen peroxide (50 μM; 15 min)-treated cells served as negative and positive controls, respectively. Panels show representative histograms, and are representative of 2 experiments.

(I) Fold-decrease in viability was calculated for MOLM13 and THP1 human AML cell lines treated with increasing concentrations of L-AA (0-1000 μM) and Olaparib (0-40 μM) for 72 hr. The dotted line indicates a fold-change of 1 in viability. Cells were assayed in triplicate at each concentration. Data are shown as mean ± SEM for 3 independent experiments.